Professorship for Polymer Engineering

Polymer Mixing in a Single Screw Extruder

Part I: Simulation Method

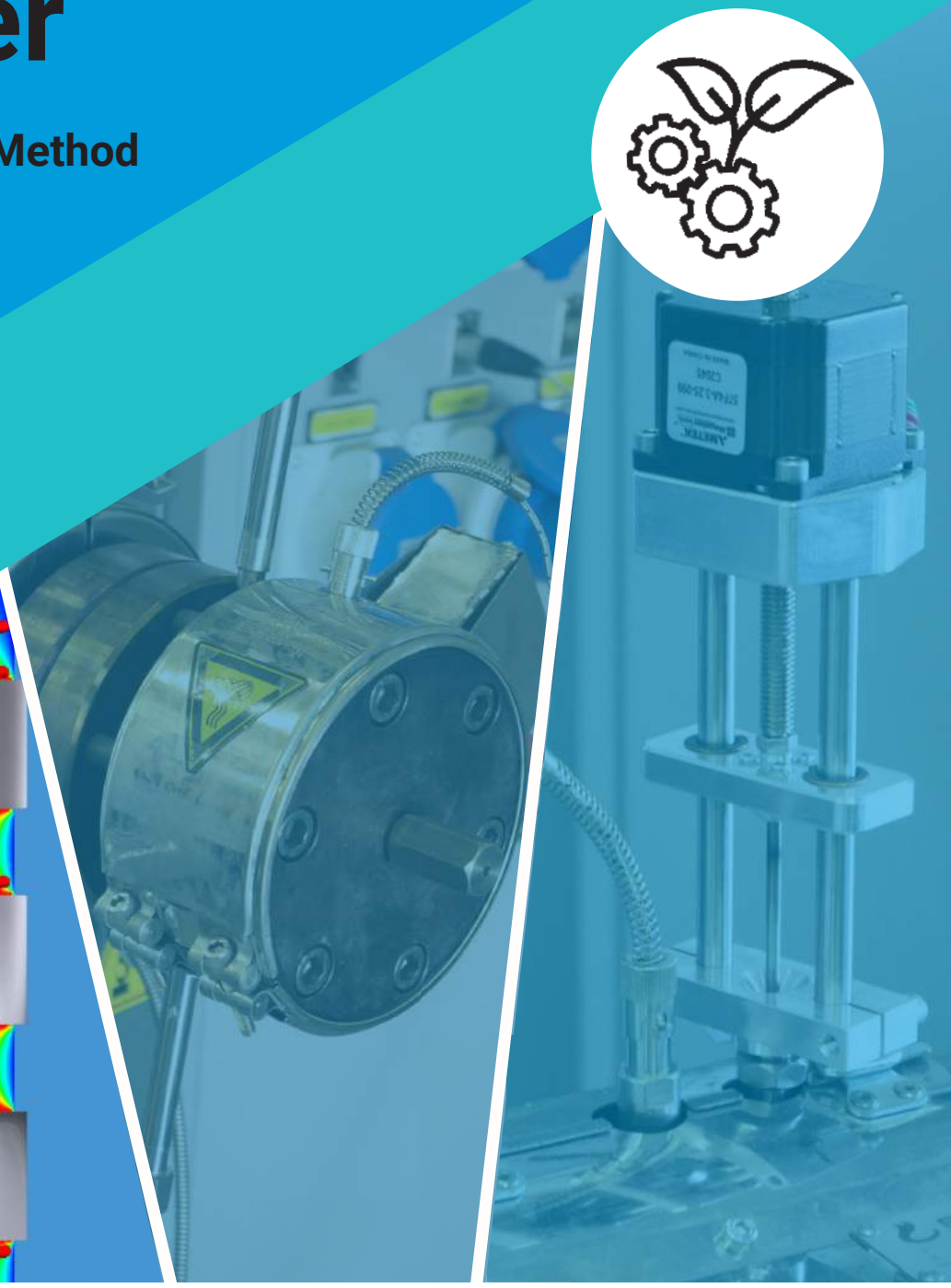

University of Applied Sciences
Windesheim

Colophon

Title: Polymer Mixing in a Single Screw Extruder (Part I: Simulation Method)

Publication number: LKT-DP-106741-2212

Publication date: December 2022

Authors: Dr. Ir. J. Buist
Dr. Ir. D.J. van Dijk
C. Hummel MSc
T.J. Mateboer MSc

Line of research:

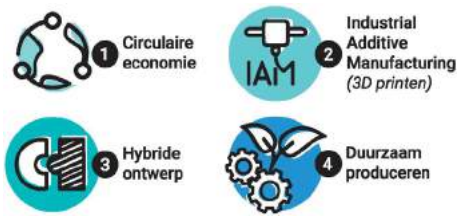

Funded by: TechForFuture

In collaboration with: Wavin T&I

This is a publication of Windesheim University of Applied Sciences and is part of Attribution 4.0 International (CC BY 4.0). This means that the content (knowledge) of this publication may be used as a base for new developments, provided that the name of the author and/or Windesheim University of Applied Sciences is stated. Company- specific data from consortium members may be omitted.

The Professorship for Polymer Engineering of University of Applied Sciences Windesheim was founded in 2009; the group's objective is to improve the knowledge base on sustainable processing of plastics and composites within and through the higher education system. Its primary function is as a research group in Polymer Engineering, delivering output in the field of applied science. Befitting research groups at University of Applied Sciences, their research spans from TRL 4 to a maximum of 7: demonstration system prototype in an operational environment.

The team operates within market based projects and comprises lecturers from Civil Engineering, Industrial Product Design and Mechanical Engineering. The output of the projects is integrated into the curriculum of these study programs.

Contents

1 Introduction

This study is part of a series of documents. This introduction contains a general preface for all documents and a specific outline of the subjects in this study.

1.1 General preface

The project 'Polymer Mixing in a Single Screw Extruder' is reported in a series of documents reporting the outcome of a four years research program, executed by the Professorship for Polymer Engineering of Windesheim University of Applied Sciences and Wavin Technology and Innovation department of the Orbia's community of companies. The project was funded by Centre of Expertise 'Tech For Future' in two successive projects, namely 'Sustainable extrusion processes in the production of pipes (TFF1703)' and 'Mixing in a single Screw extruder' (TFF1920).

Plastic pipes are commonly used for the transport of fluids. The properties of the pipe depend (amongst others) on the plastic used in the production. The properties of the plastic in their turn, can be modified with additives. For example, the color of a pipe can be adjusted by the addition of a colorant to the polymer compound. The colorants are often mixed with the polymer using specialized equipment such as twin screw extruders. However, polymer (non-PVC) pipes are generally manufactured using a single screw extruder with a pre-compounded (pre-mixed) polymer. A basic single screw extruder has poor mixing characteristics. To improve mixing, different mixing elements with different mixing characteristics (like a spiral Maddock or a pin mixer) can be added after the compression zone of the extruder. Using a combination of these mixing elements, it could be more energy- and cost efficient to both mix and extrude with a single screw extruder.

The general objective of the program was to gain detailed knowledge of the extrusion process by modern analysis tools like computational fluid dynamics (CFD). A benefit of this tool could be a shorter development time of extrusion processes. To prove the strengths of these modern tools, the optimization and selection of mixing elements in single screw extrusion was chosen as these provide a challenging case.

Based on this general objective and the specified case, the following research questions were drafted:

1. What is a proper simulation method for polymer extrusion with respect to mixing?
2. How to quantify mixing quality in an extrusion simulation?
3. How to validate the simulation results and to validate the quantification of mixing?

The basis of the study is a literature search into mixing processes in extrusion, simulation of velocity, temperature, pressure and stresses in extrusion, quantification of mixing based on flow fields in extrusion and validation of mixing in extrusion experiments. Each document contains a part of this literature search, which is relevant for the subject in the respective document.

The first document *'Simulation Method':* Different simulation techniques, with respect to the discretization method and meshing method for the rotating screw, are analysed and demonstrated for different mixing elements. The selection of a suitable simulation method is not limited to single screw extrusion because in the future double screw extrusion might also be of interest.

Preferably, a simulation method which is applicable for both single screw as well as double screw extrusion is selected.

The second document: ***'Mixing quantification':*** Several methods to quantify mixing quality were studied. In order to compare results, a method which is suitable for numerical simulations as well as for the experimental validation has to be selected.

The third document: ***'Experimental validation':*** For the study described in this paper, a single screw extruder on lab scale, with multiple monitoring points in the barrel for temperature and pressure, was acquired. The screw of this extruder has a simple basic configuration with three zones and only one mixing element. Several screws with different mixing elements are available, to be able to make a clear distinction between the various effects. The screw is easy to exchange in the extruder barrel, which makes it possible to study different type of mixing elements. The barrel contains holes that can also be used for injection of a second polymer or a colorant, for example between the compression zone and the mixing element.

Upon the completion of these research steps it should be possible to select a combination of mixing elements for an optimal mixing quality using numerical simulations.

1.2 Introduction into Simulation Method

In chapter 2 a literature search on mixing phenomena is reported. All physical phenomena, which determine mixing, are briefly discussed. These physical processes are: different types of mixing (dispersive against distributive mixing), different types of additives (colorant dyes, pigments and masterbatches) and different types of physical appearance (solid versus liquid, miscible versus immiscible polymers).

In chapter 3 the numerical simulations method is selected. First a comparison between several simulation techniques for extrusion is reported. Based on this comparison a choice was made for the numerical simulation method of mixing in single screw extruders. Preferably the choice accommodates future work like for example double screw extrusion and most of the physical phenomena from the previous chapter have to be included in the method.

In chapter 4 experiments are reported that measure the physical properties, which are needed for the simulation and experiments on a single screw extruder to validate the preliminary results of the simulation. The main physical property is the viscosity, which is temperature and shear rate dependent. The parameters for a power-law model were determined. The experiments were carried out on a small scale single screw extruder at Wavin T&I.

In chapter 5 different mixing elements are introduced with respect to suitable grid structure to obtain grid independent solutions. Only pressure, flow field and shear rates are reported. Finally, a simulation of a combination of a spiral Maddock and pin mixing element is presented because these elements have the same geometry as the experiments on the pilot extruder at Wavin T&I.

The last chapter contains the conclusion and recommendations for the next stage of the project.

2 Literature search: mixing colorants with polymer in an extrusion process

This literature report consists of several sections. Section 2.1 is a short introduction into polymer mixing, colorants and simulation techniques. Sections 2.2, 2.3 and 2.4 discuss the physics and simulations of respectively mixing solids through polymers, mixing miscible polymers and mixing immiscible polymers. Conclusions and recommendations are presented in section 2.5.

2.1 Introduction

Predicting the mixing behavior of a single screw extruder using flow simulation is the goal of the Sustainable Extrusion project. This chapter contains the results of the literature search, which forms the base of this project. The study presents the current level of scientific knowledge of the relevant subjects but the goal of this literature study is to answer the following questions:

1. What are the relevant physical phenomena involving polymer mixing processes?
2. What is the current state of the art concerning simulations of polymer mixing processes?

Polymer mixing can be done with either fluidic polymers or with solid polymers (granular mixing). This study focuses primarily on mixing of fluidic polymers. In this study a polymer is always a molten polymer if not stated otherwise.

2.1.1 Mixing: distributive and dispersive

Mixing is the process of converting a heterogeneous system into a homogeneous system. With this process entropy increases and energy is dissipated. In general three types of motion are involved in mixing: molecular diffusion, turbulence and bulk flow [1, 2]. Molecular diffusion is slow and turbulence is not present in polymer flow due to the high viscosity. Mixing polymers is therefore a result of bulk flow.

Mixing is often categorized in dispersive mixing and distributive mixing. With distributive mixing the additive units or discontinuous phase are homogeneously distributed throughout the polymer, whereas with dispersive mixing the additive units are reduced in size [3]. Increase of interfacial area is often used as a measure of distributive mixing of fluids. Increase in number of additive units is often used as a measure of dispersive mixing, see Figure 1.

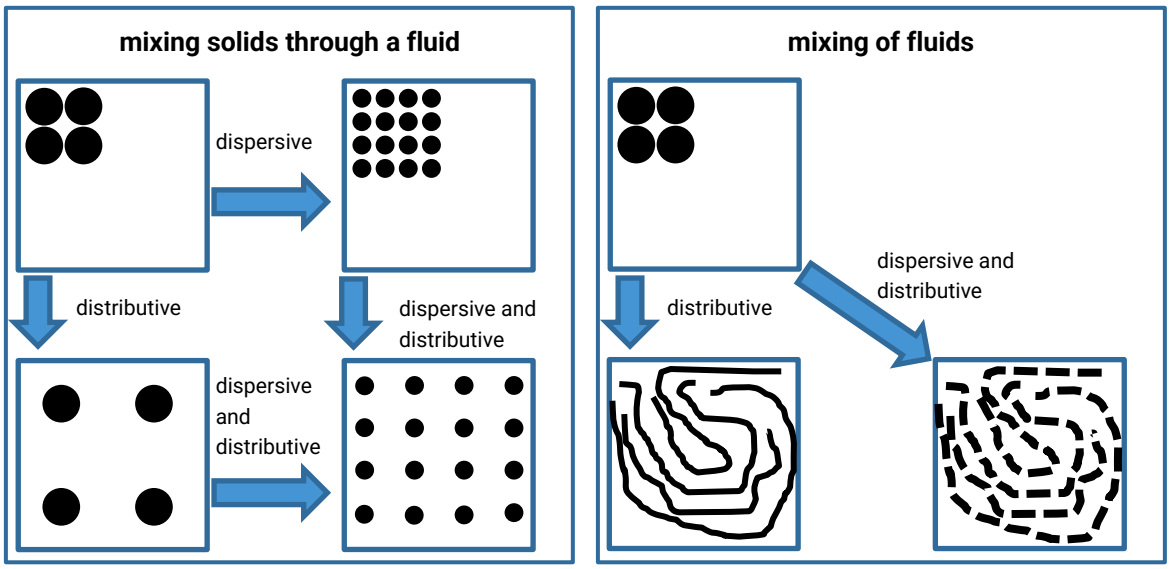

Figure 1. Schematic representation distributive and dispersive mixing. Left mixing of solids through a fluid. Right mixing of fluids.

In general, mixing is achieved with shear flow, elongational flow and chaotic flow. Elongational flow and chaotic flow are often more energy efficient in achieving a measure of mixing compared to shear flow.

2.1.2 Colorants

Colorants are additives used to internally color plastics [3]. The most frequently used polymer colorants can be categorized into pigments, dyes and masterbatches. Mixing behavior differs for each type of colorant.

Dyes are synthetic solid colorants that are soluble, and therefore easily dispersed, in polymers [3, 4]. These colorants are bright and translucent and often used in lenses.

Pigments are solid colorants that are insoluble in polymers [3-5]. Solubility is often improved by surface modification of the pigment with coupling agents. Mixing solid colorants through a polymer melt will be discussed in section 2.2.

Masterbatches are polymers with a high concentration of colorants [3-5]. Compatibilizers are often used to increase miscibility of a masterbatch with another polymer matrix. Masterbatches consist of pigments, dyes, compatibilizers and other additives and comes often in the form of pellets with a diameter of 0.35 mm up to 6 mm. It seems preferable that the polymer of the continuous phase and the masterbatch carrier polymer are compatible with each other [4]. However, often the polymer and the masterbatch carrier polymer are dissimilar. Mixing a miscible masterbatch through a polymer is discussed in section 2.3. Mixing an immiscible masterbatch through a polymer is discussed in section 2.4.

2.2 Mixing solids with a polymer

Solid colorants may be soluble dyes or insoluble pigments. The latter is the focus of this chapter. The physics behind mixing solids with a polymer will be discussed in section 2.2.1. Simulations of mixing solids with a polymer will be shown in section 2.2.2.

2.2.1 Physics of mixing insoluble pigments with a polymer

Pigment particles are often grouped in the form of aggregates and agglomerates.

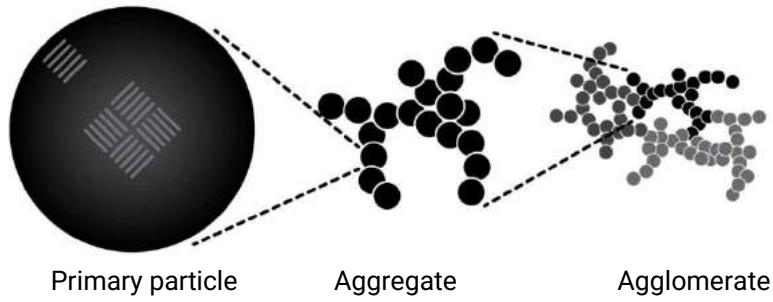

Figure 2. Schematic representation of a carbon black particle, aggregate and agglomerate. (Figure copied from reference [6])

Mixing of pigments requires dispersive mixing [7]. Agglomerates breaking up or erode due to forces acting on them [1, 8]. Breaking up of an agglomerate is somewhat similar to the breakup of droplets dispersed in a matrix fluid. Both break up due to forces acting on the agglomerate or droplet. Whereas droplet breakup is size dependent, agglomerate breakup is not dependent on size [1]. In polymer flow, two basic flow characteristics can be distinguished, shear and elongation. Elongational flow results in stronger forces acting on the agglomerate compared to a simple shear flow. Therefore elongational flow is preferable for dispersive mixing [8]. The force needed for agglomerate breakup depends on the pigment interparticle attraction. The agglomeration forces result from surface interaction involving electrostatic, Van der Waals and liquid-bridge forces. Liquid-bridge forces are a composition of capillary and viscous forces. The adhesive forces may also depend on particle shape, size, surface roughness and plasticity. The pigment particle's surface interaction with the polymer matrix has strong influence on the mixing behavior. Coupling agents are often applied to the surface of the pigment (wetting) in order to reduce the interfacial energy between the pigment and polymer. A wetting agent may also be applied to avoid interfacial attraction forces between the pigment particles [4]. This wetting also prevents reagglomeration of the particles.

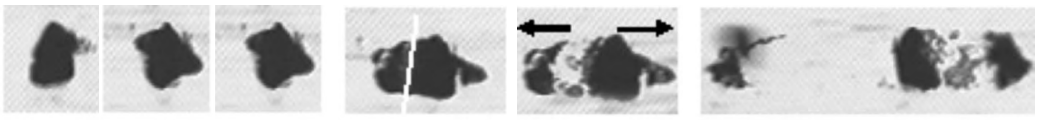

Figure 3. From left to right a rupture sequence of a carbon black agglomerate (R_0 30 µm) in a styrene-co-butadiene rubber (SBR) in simple shear flow. (Figure copied from figure 7.27, reference [1]).

Mineral pigment surfaces often have weak interaction with polymers and are often wetted before mixing with a polymer. On the other end of the spectrum are pigments like carbon black that interact with the polymer matrix and therefore often do not require wetting.

An alternative to wetting is using polymers with functional end-groups [5, 9]. The functional end group has a higher surface interaction with the pigment. Therefore the pigment disperses more easily in the polymer.

At high loadings pigments can also function as fillers, for example carbon black fillers in rubber tires. Masterbatches often have high levels of pigments, these pigments can therefore be viewed as fillers in the context of this study.

Fillers often increase the melt viscosity of polymers [5]. Fillers with a strong interaction between the particles form agglomerates and a filler-filler network at higher particle levels. These networks and agglomerates may result in an elastic behavior of the compound below a critical shear stress (Bingham fluid) whereas it behaves as a fluid at higher stresses [10-17]. The filler-filler network and agglomerates break down due to strain, this is called the Payne effect or alternatively the Fletcher-Gent effect. Breakup of the filler-filler network and agglomerates may result in a change of rheological behavior due to shear during extrusion. In other words the rheological behavior depends on the history (elastic behavior) of the filled polymer. The elastic behavior of a filled polymer inside a rheometer may differ from the behavior of a filled polymer during extrusion. This is particularly relevant with dynamic rheological measurements. Shear is low during dynamic rheological measurements and therefore minor breakup of agglomerates and the filler-filler network. This is in contrast to the extrusion process with often high shear and therefore more breakup of agglomerates and the filler-filler network. As a result there might be a discrepancy between the measured rheological behavior and the rheological behavior inside the extruder. These measured rheological parameters are however needed for extrusion simulations. A discrepancy between the two may result in a discrepancy between extrusion simulation and extrusion experiments.

Usually only a small percentage of masterbatch is used during extrusion. The local pigment density (in the masterbatch pellet) reduces quickly due to distributive mixing resulting in breakdown of the filler-filler network. Therefore the impact of pigment on the rheology will be minimal with a low amount of masterbatch.

In conclusion dispersive mixing of solids is due to high shear stress, therefore a shear stress analyses should be the focus of any dispersive mixing simulation.

2.2.2 Simulations of mixing solids with a polymer

Several studies of the mixing solids through a polymer are using numerical simulations [18-23]. Quite a few of these focus on corotating twin screw extruders [18, 19, 22] with only a few focused on single screw extruders [20, 23]. The polymer melt in these simulations are often described with a shear thinning fluid model [18-20, 22, 23]. Simulation of dispersive mixing of each solid body (similar to pigment in experiments) requires meshing of each solid body, which would result in extremely high computational costs. None of the extrusion simulation studies therefore included mixing of solid bodies in their simulations. In some of the studies a form of mesh refinement was applied [18, 20, 22, 23].

As simulation method a Finite Element Method (FEM) is frequently used for mixing simulations [18, 19, 22, 23]. In most cases Ansys Polyflow is used. One study uses a Finite Volume Method (FVM) [20]. Some studies did not include verification of the simulations with experiments [19, 20, 23] whereas other studies did verify with experiments [18, 24]. Yamada *et al.* compared the mixing behavior of several extruder segments. Both simulations and experiments showed better mixing quality for specific extruder segments. The study however did not show a quantitative validation of the simulations with respect to mixing behavior.

The distributive mixing quality in mixing simulations is often determined with RTD (residence time distribution) [19, 20, 22]. And sometimes the Shannon entropy is used as a measure of distributive mixing quality [20]. Dispersive mixing is due to agglomerate breakup which is a result of stresses working on the agglomerate. Therefore, the stresses on a particle are linked to dispersive mixing quality. The dispersive mixing quality in simulations is often determined with particle tracking [18-20, 22, 23], where the stresses acting on a particle can be evaluated. With particle tracking the path of a particle is determined based on a chosen point of entry and the velocities and trajectories that such a particle would experience. The tracer particle is a traveling point in the fluid domain, but it is not a part of the fluid domain mesh. Therefore, tracer particles do not necessarily require a large mesh. Some studies include an analyses of the elongational stretching, the shear rate and stresses working on the particle during its path through the extruder [18-20, 23]. Such analyses include the averaged, time integrated and maximum values of each determined quantity.

Slippage of the polymer melt at the wall influences the flow behavior. In a study by Chen and Cao it was found that wall slip increases distributive mixing performance but reduces the dispersive mixing [22].

Aggregate breakage, erosion and flocculation is often described with population balance equations for mixtures of polymers [25-27] or other mixtures [28, 29]. Wang *et al.* performed CFD simulations and experiments on aggregate breakup and flocculation in an aqueous solution in a Couette flow [28]. In their simulations the aggregate size was described by population balance equations. In their validation experiments the aggregate size was determined optically. It was found to be in good agreement with the simulation experiments.

In conclusion mixing of solids in a polymer can be simulated. The use of tracer particles is recommended since the particles can be used for simulating both dispersive and distributive mixing. Furthermore, the tracer particles do not inherently require a large mesh, therefore computational costs can be limited.

2.3 Mixing of miscible polymers

Thermodynamically miscible fluids are fluids with no appreciable surface tension between the fluids [30]. Miscible fluids might be a basic polymer and a masterbatch with a carrier polymer identical to the basic polymer.

Diffusion is present in miscible fluids, though very slowly due to the high viscosity, therefore diffusion is negligible during mixing and the interface between the fluids is well defined [30].

Mixing of miscible fluids is mostly a result of stretching the fluids. This is shown for a concentric cylinder mixer in Figure 4.

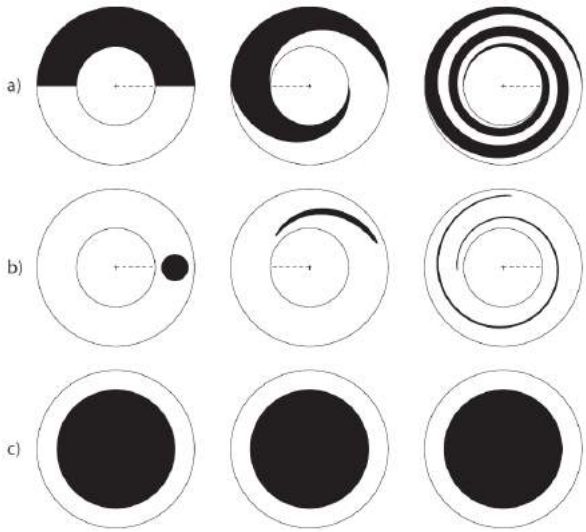

Figure 4. Mixing patterns in a concentric cylinder mixer for three different initial configurations of the two fluids. Left column: initial condition. Center column: inner cylinder rotated π radians. Right column: inner cylinder rotated 4 π radians. (Figure copied from figure 2.1, reference [30]).

Increased mixing corresponds to interface stretching [30]. Stretching within the concentric cylinder is only in tangential direction, therefore mixing is poor in radial directions. No mixing is achieved in situation *c* of Figure 4 due to the absence of stretch in radial direction.

The layers of fluid decrease in thickness with increased mixing, as is shown in situation *a* in Figure 4. The interfacial area between the two fluids increase with increased mixing. The interfacial area grows linearly with time in a simple shear flow. Exponential interfacial area growth in a confined area can be provided with chaotic flow. Chaotic flow often involves stretching and folding, see Figure 5.

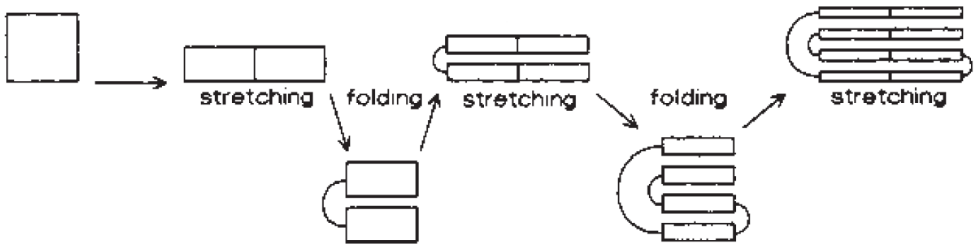

Figure 5. Efficient distributive mixing through stretching and folding leading to increased interfacial surface. (Figure copied from figure 3.5, reference [2]).

Chaotic flow results in high stretching and therefore good mixing quality. A flow with both regions of chaotic and regions of simple shear flow will however result in islands of poor mixing quality [30]. Therefore a global chaotic flow is preferable for good mixing quality.

Mixing behavior due to flow in a non-homogeneous material is often studied with analytical analyses or flow simulations [30]. The rheological properties of the two fluids may differ from each other, which may complicate the flow calculation of these mixing processes. The mixing quality or measure of mixing is often expressed in stretch ratio.

In conclusion mixing of miscible fluids is mainly due to stretching of the fluids, which results in an increase in interfacial area between the miscible fluids.

Mixing simulations with miscible fluids

Several studies focused on mixing of miscible fluids [7, 24, 31-41]. This includes studies with twin screw extruders and single screw extruders.

The different fluids, mixed in the extruder, may have different rheological properties, such as viscosity. In CFD simulations the differences in rheological properties can be accounted for with a "two phase simulation". With a two phase simulation the fluids can be separated with an interface. A fine mesh is needed for describing the thin layers of dispersed fluid due to stretching of the fluids. The computational costs of such simulations are very high due to the necessity of a fine mesh. None of the miscible fluid extrusion simulations included a two phase flow.

If both miscible fluids have the exact same rheological properties a "single phase simulation" can be used. For example, several studies of Alemaskin *et al.* [7, 35-41]. Alemaskin *et al.* studied distributive mixing ABS (acrylonitrile butadiene styrene) of two different colors with a single screw extruder, both in simulations and experiments. In the simulations the distribution of green or yellow fluid was determined with tracer particles. This approach is very similar to simulation of mixing solids in a polymer fluid, as is discussed in paragraph 2.2.2. The distribution of color particles in the simulation was in agreement with the observations in the experiments.

Zong *et al.* also used "single phase simulations" with several types of twin screw extruders in which different viscosities were assigned to different volumes of the fluid [24, 31-34]. Therefore, the rheological properties of multiple fluids can be included in the singe phase simulation. The computational costs are less since there is no need for a very fine mesh to describe the interface between the two fluids. This method is used to simulate polycondensation of PPTA (Poly p-phenylene terephtalamide) [24]. The molecular weight of PPTA increases during polycondensation and therefore its viscosity increases leading to a range of viscosities during extrusion and simulation while the material is being mixed with itself. RTD (residence time distribution) was used to compare the mixing performance of each screw. Polymer extrusion experiments (without polycondensation) were performed. Agreement was found in the RTD between the simulations and the experiments. RTD as a measure of mix quality is further discussed in part 2: *Simulation method* [42].

In conclusion mixing of miscible fluids can be simulated with a two phase or a single phase simulation. The advantage of a two phase simulations is the capability to assign different rheological properties to different fluids. But the two phase method is computational very expensive. A single phase simulations is less computational expensive and is therefore preferred. Realistic results may be found with a single phase simulation when rheological similar materials are used. Alternatively different rheological properties can be assigned to different volumes to simulate with rheologically unequal fluids but still in a single phase simulation.

2.4 Mixing immiscible polymers

Most polymers are thermodynamically immiscible [43]. Such polymer blends often have a dispersed phase (the minor component) and a continuous phase (the major component). During mixing the dispersed phase is stretched which results in distributive mixing. Threads and droplets of the dispersed phase may breakup at high stress (τ), hence dispersive mixing. An example of both thread breakup and droplet breakup is shown in Figure 6. The breakup of threads and

droplets does not happen with miscible fluids. This is a key difference in the mixing behavior between miscible and immiscible fluids.

Stress on threads and droplets results in the deformation and elongation. Spherical droplets deform into ellipsoids. The surface tension has a profound influence on mixing behavior [1, 43-45]. The surface tension (v) counteracts the deformation. As the thread or droplets extend, the diameter is reduced until shear forces no longer dominate the surface tension and the thread or droplet breaks up.

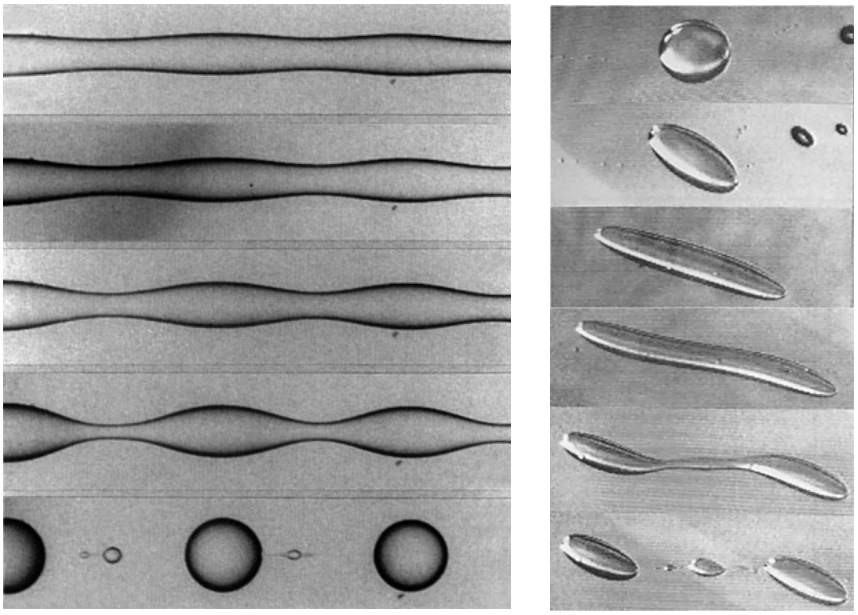

Figure 6. Left: from upper to lower image thread breakup (diameter 55 µm) of PA6 in a PS matrix at 230 °C. Right: from upper to lower image droplet breakup of a Newtonian fluid in simple shear flow. (Left figure copied from figure 7.24, reference [1]. Right figure copied from figure 3.64, reference [43])

The ratio between the shear stress and the interfacial stress (σ/R, R is the local radius) is called the capillary number (κ) [1, 2, 8, 43, 44, 46].

$$\kappa = \frac{\tau R}{\sigma} \qquad 1$$

The droplet and threads breaks up if the capillary number exceeds a critical value (κ_{cri}). After droplet breakup the capillary number decreases due to decreased droplet size. The dispersed threads and droplets do not break up but only deform if the capillary number is below the critical capillary number.

Breakup of a droplet is somewhat similar to the breakup of agglomerates, see section 2.2 and is the result of shear or elongational flow. However, droplet breakup is size dependent (see equation 1), while agglomerate breakup is not dependent on size [1].

Droplet coalescence may happen in regions with low shear stress. The average droplet size characterizes the mixing process as it is the result of a dynamic equilibrium between droplet breakup and coalescence.

Immiscible fluid mixing can be divided into:

1. distributive mixing at ($\kappa<\kappa_{crit}$) with mainly stretching of droplets and threads but no droplet breakup due to the high interfacial stress compared to the shear stress
2. dispersive mixing at ($\kappa\approx\kappa_{crit}$) with droplet breakup and increase in number of droplets due to the high shear stress compared to the interfacial stress

The critical capilary number, κ_{crit}, depends on the type of flow and on the viscosity ratio ($\lambda=\eta_{dispersed}/\eta_{matrix}$). In simple shear flow the stress is partially used to rotate the droplet. In elongational flow the complete stress is used to deform the droplet. Therefore, elongational flow is more efficient for dispersive mixing. Grace found that droplet breakup is possible at a viscosity ratio of 10^{-6} up to 3.5 in shear flow [46]. The lowest critical capillary number was found in the viscosity ratio range of 0.1 up to 1.0, see Figure 7.

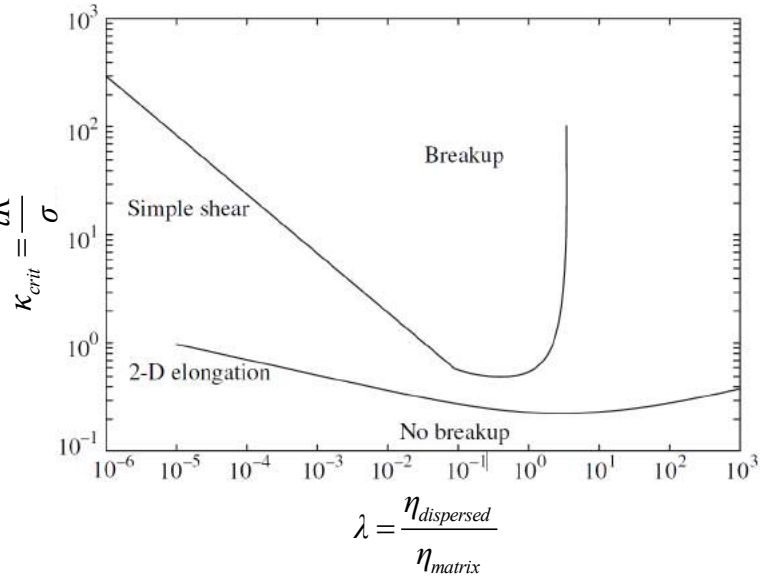

Figure 7. Critical capillary number for droplet breakup in shear and extensional flow (Figure copied from figure 7.23 of reference [1]). [8, 44, 46]

Viscoelastic effects of the fluids may result in easier breakup of threads [43]. The breakup of droplets is however less dependent on viscoelasticity and coalescence is retarded by viscoelasticity.

Simulations of immiscible polymer mixing

The Boundary integral method (BIM) is applied in several studies to simulate droplet breakup and coalescence [43, 47]. The droplet surface is divided into several mesh elements and remeshing is applied to each droplet. This method is applied in simulations with a very low number (single digits) of droplets. As a result, this method is too cost intensive for larger systems like a whole extruder.

Simulating individual droplets can be avoided with a two zone model or by implementing population balance equations (PBE) [43, 48-50]. A two zone calculation consists of a strong and a weak zone. In a strong zone both threads and droplets are stretched and broken up. In the weak zone threads may breakup but droplets may coalescence. The computational costs are less with PBE since not each droplet is meshed.

PBE are used to describe breakup and coalescence of droplets. Population balance models have been used in several CFD simulations studies with low viscosity Newtonian fluids (fluids other than polymers) [49, 50]. The population balance model tracks the droplet number density, the droplet size, the rate of droplet breakup and droplet coalescence. Therefore, PBE are recommended to use with simulations of immiscible polymer mixing in an extruder.

2.5 Conclusion and recommendations

This literature study is focused on the physics of polymer mixing with an extruder and CFD simulations of this process.

The relevant physical phenomena involving polymer mixing were studied. Colorants are often solid pigments or masterbatches of polymers with pigments. Mixing colorants with polymers can be divided into three categories: mixing solids with a fluidic polymer, mixing miscible fluidic polymers and mixing immiscible fluidic polymers. Theoretically, mixing can be achieved due to molecular diffusion. However, this phenomenon is negligible with polymers due to their high viscosity. The mixing process is often divided into two components. First, in distributive mixing the dispersed units become more homogenously scattered through the matrix polymer. Then, secondly, in dispersive mixing the number of dispersed units increase. Dispersive mixing is present when droplets or threads breakup in an immiscible mixture or when solid aggregates erode or breakup.

A great number of studies focused on simulations of a polymer mixing process. It was found that simulating individual droplets or aggregates requires a very dense mesh leading to extremely high computational costs. Simulating each droplet or aggregate is circumvented by implementing population balance equations. These are used to describe breakage and coalescence of droplets or the breakage, erosion and flocculation of agglomerates. Distributive mixing of multiple polymers is due to stretching of both the dispersed and the continuous phase. A two phase simulation with both fluids requires a very dense mesh in order to simulate such thin threads and droplets. Computational costs are extremely high when simulating with such dense meshes. Most simulation studies therefore do not use a two phase setup. Nor is the influence of dispersive mixing of solids on the rheological behavior of the fluid included in the simulations. With these studies only a single fluid is included, a strategy that might be valid in specific situations. For example Alemaskin *et al.* simulated mixing of miscible polymers. These polymers have very similar rheological behavior and can therefore rheologically be viewed as a single fluid.

Because the flow and mixing behavior of polymers are complex, extrusion simulations are complex as well. With simulations it is often recommended to start as simple as possible, and if needed to add more complexity. It is specifically recommended to start extrusion experiments and simulations with miscible polymers with a similar rheological behavior (single phase simulation). This reduces complexity since droplet breakup and coalescence are excluded and, as a result, computational time is less than compared to a two phase simulation.

It was found that no simulation studies included the viscoelastic behavior of polymers and seldom included wall slip. However, in one particular study it was found that wall slip should not be discounted as it does influence the mixing behavior of the extrusion simulation. Many studies also do not include any temperature dependent rheological behavior of the polymer. Rheologically complex fluids (viscoelasticity, wall slip, temperature dependence) are difficult to characterize and to implement this behavior in simulations. Therefore, it is recommended to use polymers with minimal elastic properties, wall slip and temperature dependence at extrusion temperature.

Some studies made a comparison between simulation and experiment. Zong *et al* studied mixing and found agreement in the residence time distribution of experiments and simulations. For most other studies the comparison between simulation and experiments is qualitative and not quantitative. Some studies also compared simulation and experiments based on parameters that are not linked to mixing quality. In these particular cases simulations were verified without verifying the mixing itself. It is recommended to verify mixing simulations with mixing experiments, methods to quantify mix quality are discussed in part 2: *Mixing quantification* [42].

3 Numerical Method: Theory and Selection

The goal of the project is to generate a simulation procedure for polymer extrusion. Several simulation techniques are available for extrusion simulation, see chapter 2. In literature no solid arguments are found which simulation technique is the most suitable for investigating mixing in single screw extrusion. Therefore several methods are described in section 3.1 and in section 3.2 a selection will be made which technique will be used in the project.

3.1 Comparison between several extrusion simulation techniques

Several simulation methods have been studied in order to determine which method is best for extrusion simulations. With respect to numerical techniques in extrusion simulation two major aspects have to be discussed. Firstly an extruder has a rotating part, the screw, and a stationary part, the barrel and secondly polymers are in principle viscoelastic materials. The models for these aspects have to be possible in the discretization technique and also have to be implemented in the available software.

In our research study two different simulation packages were used with different discretization methods: Ansys Polyflow and Ansys CFX. Polyflow is a finite element method (FEM) and is often used for non-Newtonian, laminar flow simulations like polymer processes. CFX is a finite volume method (FVM) and is most often used for Newtonian, turbulent flow simulation. CFX is strong in simulation of rotating machinery, like pumps, compressors, or turbines. It is not known how this method performs in polymer extrusion simulation.

Two methods for rotating models (to simulate a rotating screw) are available in both packages: the Sliding Mesh Interface (SMI) and the Immersed Solid Method (ISM), also called the Immersed Boundary Method (IBM). An introduction into the discretization techniques (FEM and FVM), and the rotating models (SMI and ISM) is given in section 3.1.1 Also, the possibility and need for a viscoelastic model is discussed.

Simulations with the different discretization techniques and rotating models were performed and compared in order to determine which method is best for extrusion simulations. The preferred simulation method gives accurate results, has low computational costs and has a short calculation time. Furthermore, the time needed for creating a mesh and setup is a relevant parameter. The simulation setups are shown in section 3.2.1, and the results in section 3.2.2.

Introduction into numerical techniques

In this section the discretization of the balance equations is given for the available software within our group. Different models for rotating machinery are presented. Shortly, the possibility and need for a viscoelastic model is discussed.

3.1.1 Discretization and available software

In chapter 2 the results of several simulation articles were discussed for mixing in extrusion processes. In most literature the numerical method was hardly mentioned, validation of the results is poor and no qualitative or quantitative comparison between the methods is found.

The performance or accuracy of the finite element method and finite volume method are difficult to compare. The reason lies in the different approaches of discretization. Also, hardly any literature can be found on a comparison with respect to accuracy, stability, robustness and ease of use. An extensive explanation of the differences can be found in [54], where the methods have been applied to natural ventilation in greenhouses. Here, the essence of these two methods will be briefly discussed and more importantly, the consequences with respect to the mesh requirements, computation time and memory requirements.

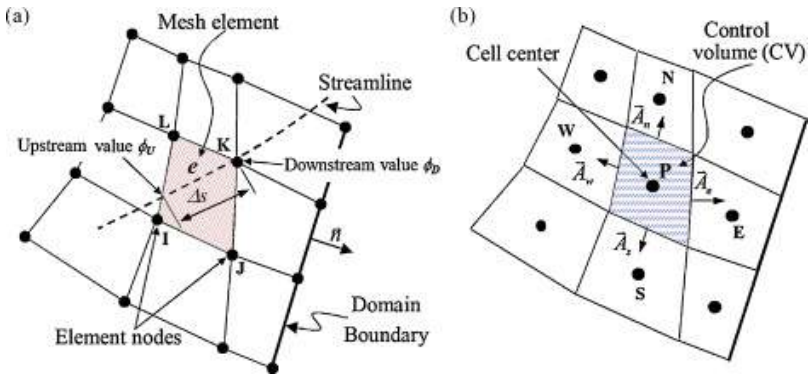

Figure 8. A representation of a structured mesh for the two discretization methods. Left (a): finite element method. Right (b): finite volume method (Figure copied from Figure 2, reference [54]).

The balance equations for mass, momentum and energy are solved by dividing the fluid domain in a number of elements. In the finite element method, the variables, like velocities, pressure and temperature, are interpolations of local polynomials or shape functions of the values of the variables at the corner points. The weighted residuals are obtained by multiplying the equations with so called weighting functions. This set of equations is integrated over the entire computational domain. Several choices can be made for the shape functions and weighting functions [55]. In the finite volume method, the balance equations are integrated in each cell by volume integrals. After the formulation of these volume integrals and applying the divergence theorem, the integration reduces to surface integrals. Then, the second order differential equation reduces to a first order differential equation [56]. The first order derivatives are evaluated using differential schemes, based on Taylor expansion of the values at the cell centers. Generally speaking, the FVM is a special case of FEM, when the weighting functions are equal to one [54].

In principle the same numerical grid can be used for the finite element method as for the finite volume method. But, comparison of the results obtained with the same grid for both methods is meaningless. Due to a larger number of freedom in an element, the grid for a finite element method is allowed to be much coarser to obtain comparable accuracy. As a consequence, the results have to be compared based on memory usage and computation time, assuming converged results.

An advantage of FVM is that mass is conserved, since the flux entering a given volume is equal to the flux leaving the adjacent volume. This makes this method less sensitive to numerical dispersion, which increases with finer meshes. Whether this phenomenon is of relevance in mixing of polymers in the laminar flow regime is not clear. In some cases the finite element method is sensitive to numerical dispersion.

Finally, the software package Ansys CFX uses a coupled solver, which makes the iteration process robust. In Ansys Polyflow evolutions schemes might be needed, which takes time to find a proper variable to apply in the evolution process or a converged solutions is difficult to obtain.

3.1.2 Rotating model

The most frequently used numerical techniques for rotating models are the Sliding Mesh Interface (SMI) [57, 58] and the Immersed Solid Method (ISM) [59, 60]. The SMI model is used in a Rotating Frame of Reference (RFR), the ISM model will rotate the solid only.

The SMI model makes use of a cylindrical region around a rotating rigid model. The region around the RFR is stationary, this will result in two regions with sliding interfaces in between them (Figure 9).

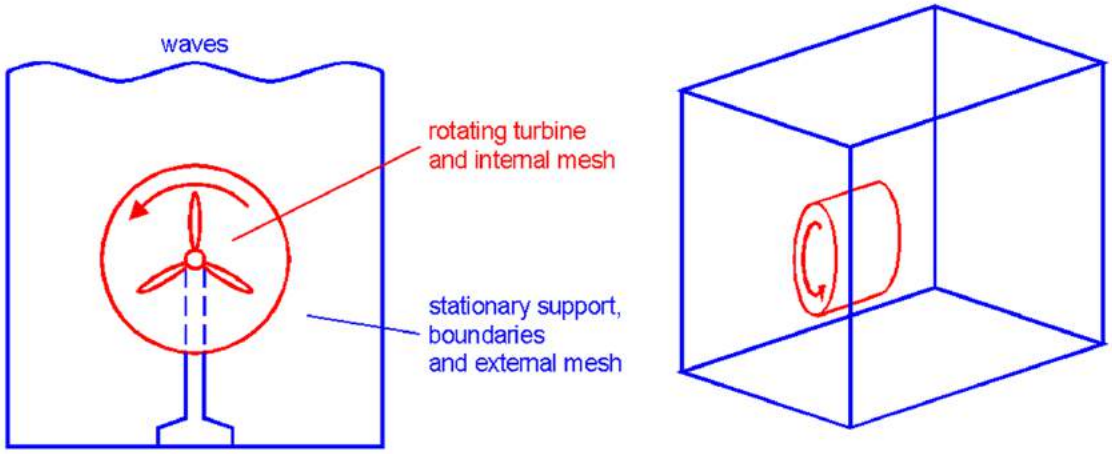

Figure 9. Rotating internal mesh in the RFR and stationary external mesh, with a SMI (Figure copied from Figure 1, reference [57])

The interfaces and therefore their nodes of the regions are sliding. This will result in none overlapping elements (Figure 10) which can result in disturbance of the physics at the transition of the rotating and the stationary domain. In reality this disturbance is absent, it should be minimized as much as possible. There are solutions for this, but these will result in longer calculation times [57, 58]. However, this method does not need a lot of mesh refinement which reduces calculation times.

The rotating mesh is modeled onto the geometry of the rotating body, i.e. the screw. A change of the screw geometry requires a new mesh. This cost a significant amount of working hours and processing time if many different screws are simulated for a comparison in extruder mix quality.

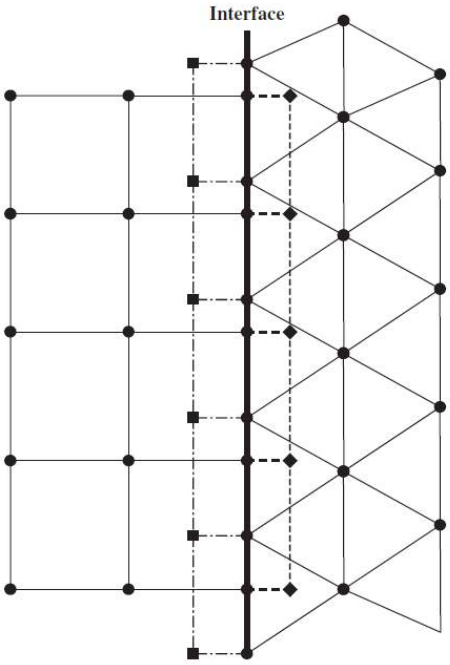

Figure 10. Sliding of the moving mesh on the interface of the stationary mesh will result in none overlapping elements, with a SMI (Figure copied from Figure 1, reference [58])

The ISM makes use of a solid and fluid region. The solid region rotates in the mesh of the fluid region. The elements inside the solid region are not used. The actual shape of the solid is created by the nodes which are closest to the interface of the solid (Figure 11) and can change while rotating (the mesh of the fluid is not rotating). Therefore, a fine mesh next to the interface of the solid is needed. A bigger region of mesh refinement is needed if the solid is not shaped like a circle. These high mesh refinements will result in long calculation times for this method. An inflation layer on the interface is also needed when the transition of velocity is big at the interface. Keeping this inflation layer intact on the interface of the solid requires a very complicated remeshing technique, which will result in even longer calculation times, therefore the use of an inflation layer should be avoided with ISM whenever possible. An inflation layer is needed with turbulent flows (big transition of velocity). However, an inflation layer is not needed for a laminar flow like the flow in an extruder for polymer processing, therefore ISM can be a good numerical technique for the simulation of mixing inside an extruder. Shear thinning fluids however will result in a bigger transition of velocity and may or may not need an inflation layer.

The fluid domain and the solid domain are meshed independently of each other. Changing the screw geometry would only require remeshing the solid domain. Meshing the solid domain is not as computational expensive as in the case of the fluid domain. The solid domain mesh only needs to describe the solid surface, large mesh elements are suitable for surfaces with a small curvature and for the inside of the solid body. Therefore, simulating and meshing many different screw cost less working hours and computational costs compared to the SMI. Especially since meshing is not easy to parallelize (using multiple processors), and therefore central processing unit (CPU) time translates to a lot of real time.

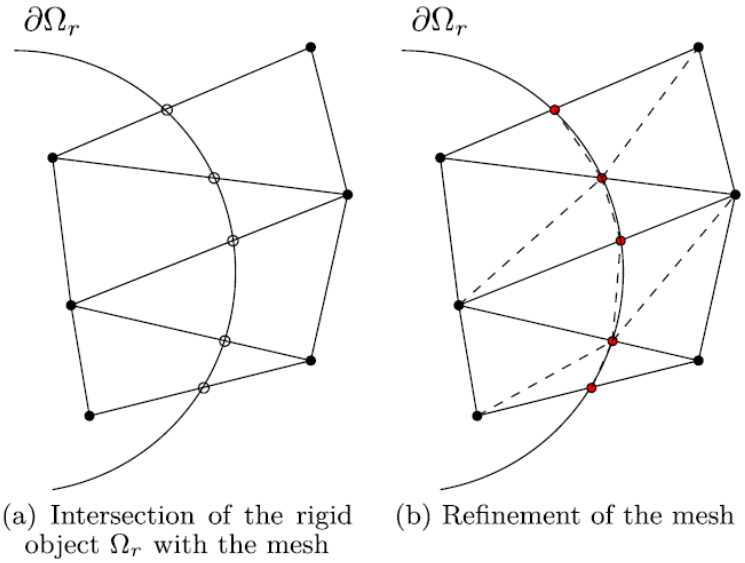

Figure 11 ISM needs local refinement of the mesh at the interface of the immersed solid (Figure copied from Figure 1, reference [59])

As mentioned, a remeshing technique may be needed with the use of ISM resulting in long calculation times. A less time consuming option is the Mesh Superposition Technique (MST). This method only divides an element into 4 elements when refinement is needed (Figure 12). In subsequent steps newly refined elements can again be divided into 4 elements if needed. This way the rest of the mesh does not require remeshing, resulting in a less time consuming method [61].

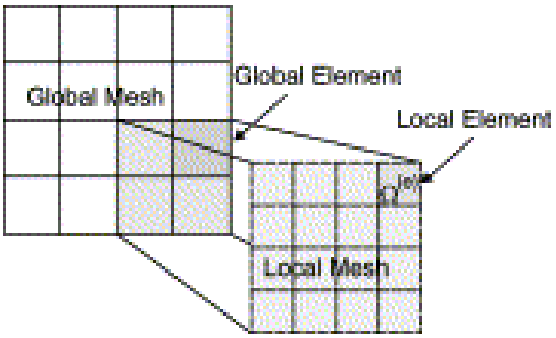

Figure 12. MST used for local refinement of the mesh (Figure copied from Figure 1, reference [61])

In conclusion both ISM and SMI can be used to simulate mixing in an extruder. SMI can have inaccuracies at the sliding interface and ISM can have inaccuracies at the interface of the immersed solid. These inaccuracies can be reduced with an increase in mesh density near the sliding mesh interface for SMI or, with the ISM, the region where the solid rotates. This is more favorable for SMI since a far larger region needs a fine mesh with the ISM. The impact of these inaccuracies may be determined with a mesh study. Comparing these results with measurements is necessary for verification. To simulate the mixing process of a twin screw extruder, ISM is the only technique that can be used since SMI is not suitable for two intersecting rotating mesh regions. Therefore, the ISM is preferred for possible future work on twin screw extruders. Furthermore, the costs are less when comparing many different screws with the ISM compared to the SMI.

3.1.3 Viscoelasticity

Modelling viscoelasticity in polymer flow is rather complex but in some cases unavoidable. For example, dye swell is mainly due to viscoelastic effects. Simulation of these effects is limited to simple geometries and simplified viscoelastic models with reasonable computation time. Simulations of dye swell in rubber extrusion showed that a structured mesh of hexahedral elements was needed to achieve convergence [62]. In this study Ansys-Polyflow was used. However, in the pressure zone of the extruder, the mixing elements behind the pressure zone and in the head/dye of the extruder, the viscoelastic properties are limited since the polymer is fully melted and the temperature is higher than the melting temperature. Therefore, the viscosity can be modelled with a generalized Newtonian viscosity model, which is available both in Ansys-CFX and Ansys-Polyflow.

3.1.4 Conclusion

The SMI and ISM are available for single screw extrusion. SMI can have inaccuracies at the sliding interface and ISM can have inaccuracies at the interface of the immersed solid. These inaccuracies can be reduced by applying an increased mesh density in those areas. This is more favorable for SMI since a smaller region requires a fine mesh. The impact of these inaccuracies may be determined with a mesh study. Comparing these results with measurements is necessary for verification.

To simulate the mixing process of a twin screw extruder in the future, ISM is the only technique that can be used. Furthermore, the costs are less when comparing many different screws with the ISM compared to the SMI. In section 3.2 the ISM and SMI methods are compared for single screw extrusion. When the performances of both methods with respect to accuracy, computational costs and user friendliness are comparable, the ISM method is preferred in supervising future work.

To simulate mixing in extruders both FVM (Ansys-CFX) and FEM (Ansys-Polyflow) are available. The performance and accuracy of these methods are difficult to compare due to differences in discretization. Therefore, these methods must be compared in a specific extrusion case, based on memory usage and computation time, assuming converged results.

3.2 Selection of simulation technique for extrusion

In this section the numerical methods (SMI and ISM) are compared with Ansys CFX as well as with Ansys Polyflow.

3.2.1 Simulation setup

4 types of simulations were performed to find the most suitable simulation technique. The simulations were performed with Polyflow as well as CFX. For both packages the SMI method as the ISM method were used. The same geometry, boundary conditions and generalized Newtonian models were used for each simulation. To compare the different numerical methods, a single screw extruder without mixing element was used. The extruder geometry and boundary conditions are presented in section 3.2.1.1.

3.2.1.1 Extruder geometry and boundary conditions

The simulation geometry consists of the metering section of an extruder screw, a torpedo and a die for tube extrusion. The geometry is shown in Figure 13.

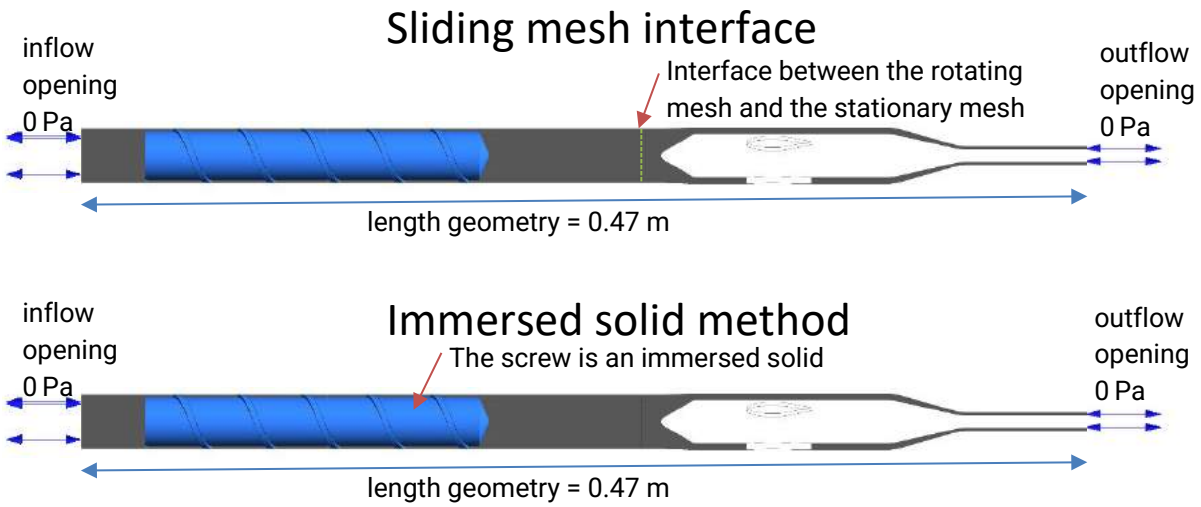

Figure 13. Upper image: Simulation geometry for sliding mesh interface simulations. Lower image: Simulation geometry for the immersed solid method simulations.

There is some space between the inflow opening and the extruder screw in order to prevent numerical instabilities. A 0 Pa boundary condition is set at both the inflow opening and the outflow opening. The screw rotates at 10 rpm.

3.2.1.2 Mesh

Both simulation quality and computational costs depend on mesh size. Ansys Meshing was used to make several different meshes for each simulation method. In general, the outcome of simulations with a coarse mesh are often incorrect. A mesh is considered fine enough when the simulation results do not change with an increase in mesh size. A mesh template was created for each simulation method. This template was used to make relatively fine meshes and coarse meshes. Each mesh from the template has the same mesh cell aspect ratio and a fixed increase in cell size over a distance. This allowed a comparison of simulations with the same setup and mesh type, but with a different mesh cell density. Most of the mesh cells are stretched out along the flow direction. The simulation geometry is divided into 80 bodies for CFX SMI, 54 bodies for CFX ISM, 71 bodies for Polyflow SMI and 35 bodies for Polyflow ISM. This division allows for a structured hexagonal mesh in a large part of the geometry and better control of the mesh setup.

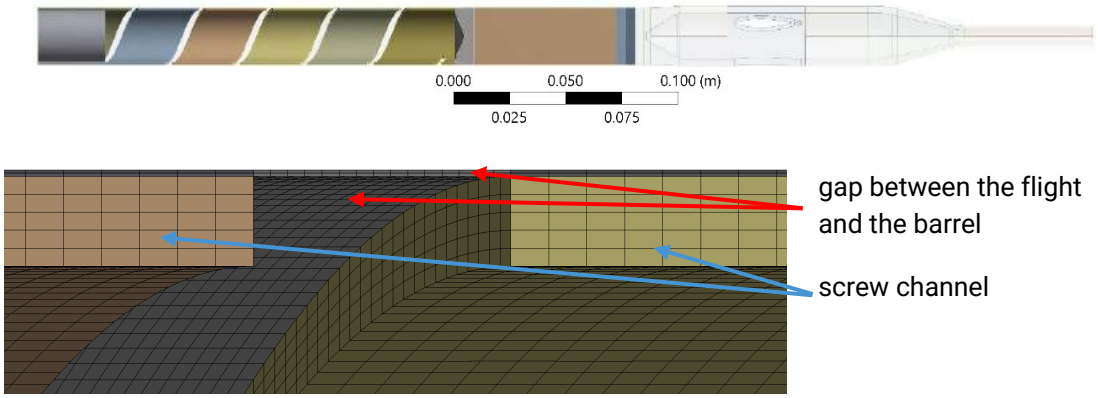

Figure 14. Upper: Cross section of the CFX SMI bodies used for meshing. Lower: part of the CFX SMI extruder mesh with 5 cells across a gap.

The bodies used for the mesh include several bodies placed between the screw flight and the barrel wall. A minimum number of cells across a gap was used for each mesh, see Table 2. This results in very small mesh cells in areas such as the gap between the screw flight and the barrel. Four meshes were made for each simulation technique in CFX and two meshes were made for each simulation technique in Polyflow see Table 1. The number of elements needed for a reliable simulation in FEM (like Polyflow) is less than the number of elements needed for a reliable simulation in FVM (like CFX). Polyflow for instance becomes less stable at a high number of elements. For these reasons the difference and amount of variation in mesh size in CFX is bigger than the difference and amount of variation in mesh size in Polyflow. Dividing the geometry into several bodies for meshing gives more control over the mesh, but it is a very time consuming process.

Table 1. different mesh sizes in million elements (M)

Cells across a gap		CFX number of elements		Polyflow number of elements	
Screw channel	**Screw flight**	**SMI**	**ISM**	**SMI**	**ISM**
5	4			0.48 M	0.53 M
	5	2 M	3 M		
8	6			0.78 M	0.69 M
	10	14 M	21 M		
	15	49 M	80 M		
	20	106 M	169 M		

3.2.1.3 Fluid model

The fluid model is based on Marlex TRB-432 (Chevron Phillips Chemical Company), a bimodal HDPE grade often used for pipe extrusion. The HDPE was rheologically characterized with a capillary rheometer, as shown in section 4.1. The power law constants are n=0.346 and m=3.29·10^4 Pa·s^{-n} with a density of 760 kg/m^3 at 200 °C.

3.2.1.4 Time step size

The performed simulations are transient. Each consist of series of simulations with time step t between each simulation. Transient simulations with particle tracking with a Courant number (C) of $C \leq 1$ are usually less sensitive to numerical instabilities. Therefore, a maximum Courant

number of 0.5 was chosen. The timestep size can be calculated with the *C*, the mesh cell length (*l*) in the flow direction, and the fluid velocity (*u*):

$$t = \frac{Cl}{u} \qquad 2$$

A smaller mesh cell size results in a smaller time step. This in turn results in longer calculation times. The timesteps are shown in Table 2.

Table 2. time step

Mesh	Time step (s)
CFX SMI 2 M	1E-02
CFX SMI 14 M	6E-03
CFX SMI 49 M	4E-03
CFX SMI 106 M	3E-03
CFX ISM 3 M	1E-02
CFX ISM 21 M	6E-03
CFX ISM 80 M	4E-03
CFX ISM 169 M	3E-03
Polyflow SMI 0.48 M	5E-02
Polyflow SMI 0.78 M	5E-02
Polyflow ISM 0.53 M	5E-02
Polyflow ISM 0.69 M	5E-02

3.2.2 Results

Simulations were performed with different methods to find the most suitable simulation method and mesh size. The different simulations were assessed by comparing the simulated pressure, flow rate, velocity profile and calculation time.

The pressure inside the extruder and the flow rate are parameters that reflect the simulation as a whole. The pressure gradient in the extruder is similar between the different simulation methods, see Figure 15.

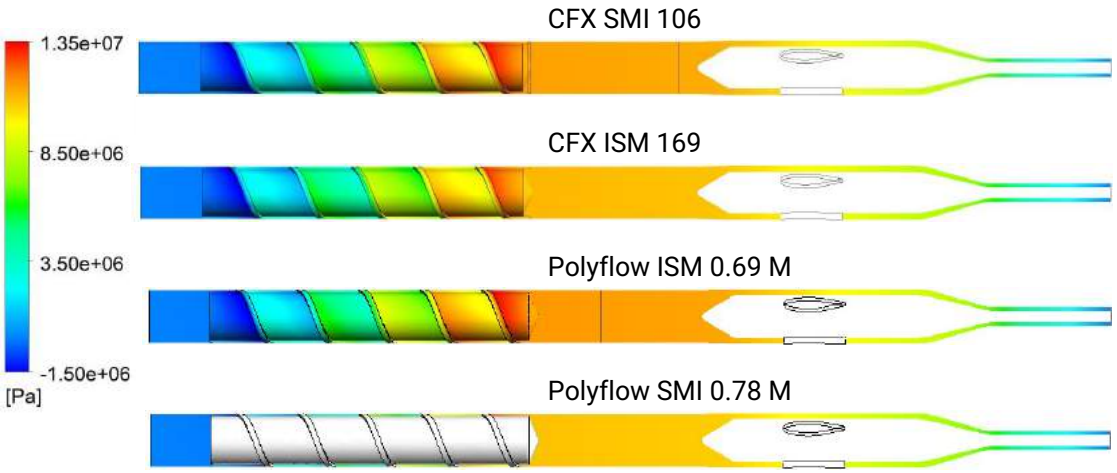

Figure 15. Pressure gradient in the CFX SMI 106 M, CFX ISM 169 M, Polyflow SMI 0.78 M and Polyflow ISM 0.69 M simulations.

Pressure and flow rate were compared to determine the adequate mesh size. The pressure in the simulation was determined at a point between the extruder screw and the extrusion die, in a region with a small pressure gradients.

Figure 16. Cross section of the simulation geometry. The pressure was determined at the red square.

The pressure and flow rate as function of mesh size are shown in Figure 17.

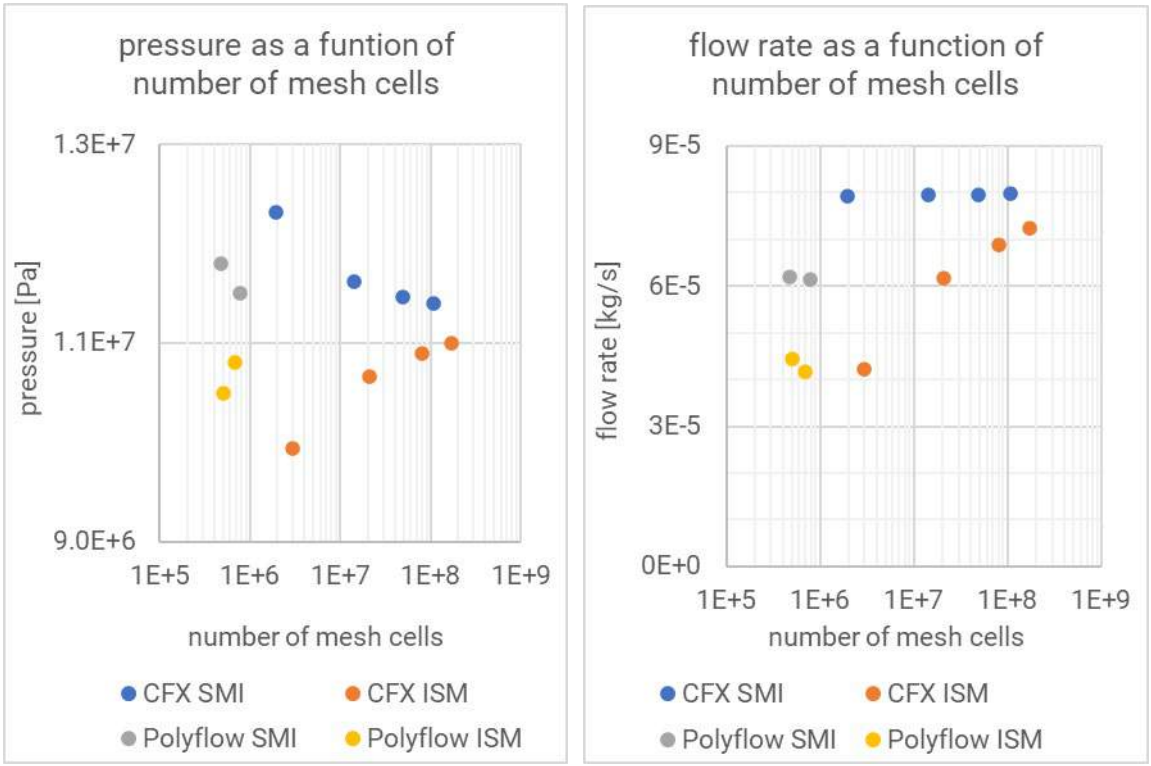

Figure 17. Left: pressure as a function of number of mesh cells. Right: flow rate as a function of mesh cell.

Pressure and flow rate for both CFX SMI and CFX ISM show little mesh dependency at a high number of mesh cells. Therefore, the CFX SMI mesh with 49 M cells and the CFX ISM mesh with 80 M cells are large enough for extrusion simulations. With a high number of mesh cells, the difference in pressure between all 4 methods reduces to a maximum of 0.7 MPa. The average pressure drop in the extruder is 11.2 MPa. SMI shows a higher flow rate than ISM with both CFX and Polyflow. The difference in flow rate between CFX SMI and CFX ISM reduces to 9 % with a finer mesh. The difference in flow rate between Polyflow SMI and Polyflow ISM does not reduce with the finer mesh.

For a more in-depth comparison the pressure alongside the barrel wall is shown in Figure 18.

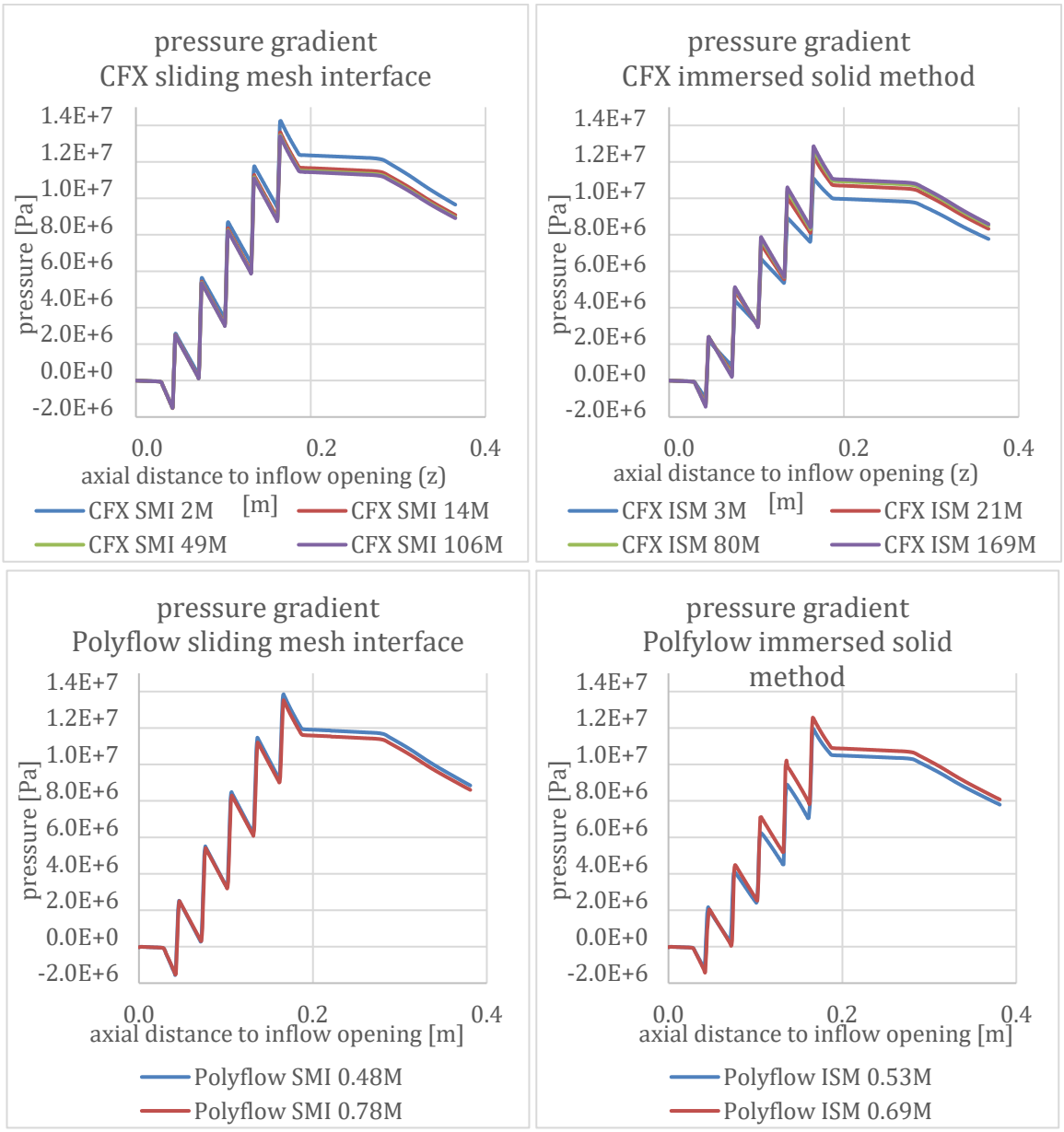

Figure 18. Pressure as a function of axial distance. Left: SMI. Right ISM. The pressure drop inside the die is not included in these graphs.

In this simulation all the pressures should be viewed as a pressure relative to the boundary conditions. In an extrusion experiment the outflow pressure is in the range of ~ 10^5 Pa, therefore a pressure of less than 0 Pa is the result of the simulation setup, not a physical phenomenon.

The die only consumes pressure and therefore shows a downward pressure slope. Due to the pumping action of the screw the pressure gradually increases in the extruder up to the end of the screw. The pressure also shows a sawtooth like profile along the screw. Two types of regions can be identified along the screw: a region with a downward pressure slope (0 > dP/dz), this is along the width of the screw channel. And a region with an upward pressure slope (0 < dP/dz), this is in the gap between the screw and the die. There is a significant pressure difference over the screw flight.

The different meshes, with the same simulation method, show mostly a difference in the extrusion die (>0.2 m) and less in the screw channel, especially with SMI. This might be due to the difference of velocity profile in the screw and in the die. In the screw channel is mostly a shear flow with a linear velocity profile, while a pressure flow is inside the die, with a curved (almost parabolic) velocity profile. Less elements are needed for describing a linear profile compared to a curved profile.

Figure 19 shows the axial velocity profile of a CFX SMI, a CFX ISM, Polyflow SMI and a Polyflow ISM.

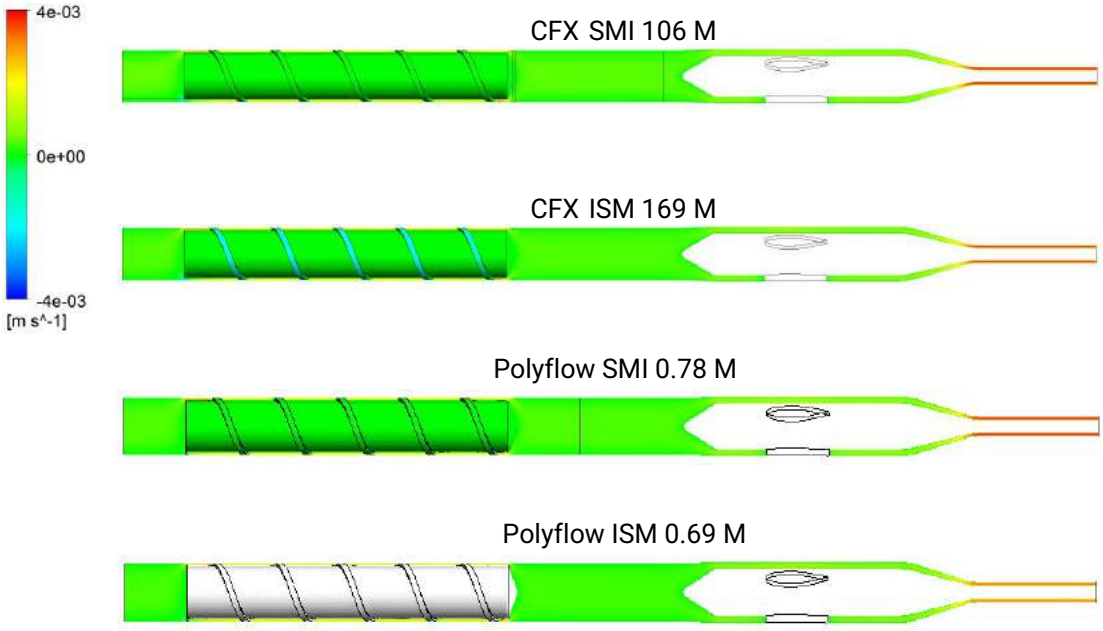

Figure 19. Axial velocity profile inside the extruder.

The velocity profiles of the SMI and ISM simulations are similar. The flow rates of the SMI simulations are a little higher, therefore the velocity is also a little higher in areas such as the extrusion die. There is some backflow between the screw flight and the barrel, see Figure 20.

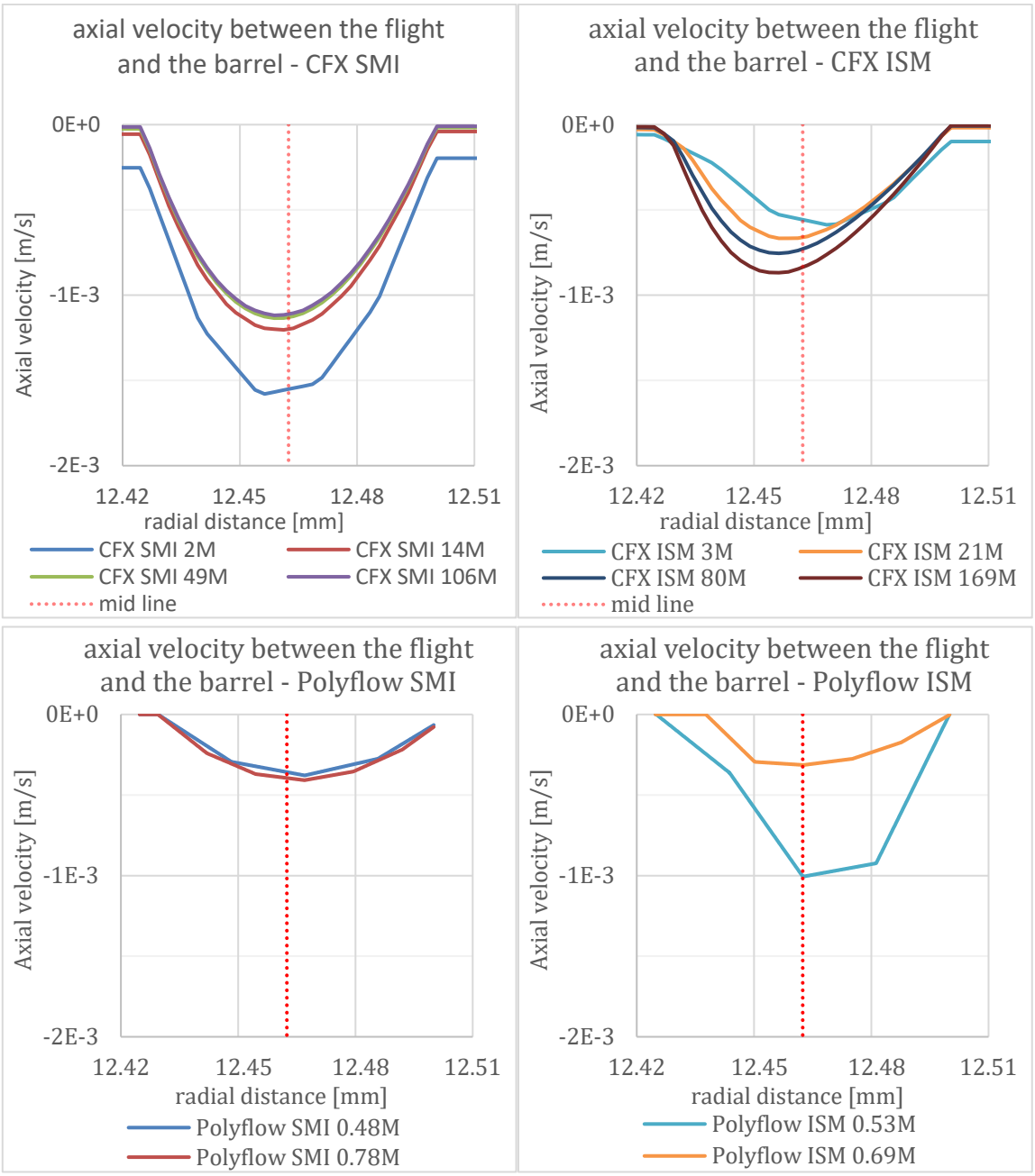

Figure 20. Axial velocity between screw flight and barrel. The red dotted line shows the middle between the screw flight and the barrel. Left: SMI. Right ISM.

As can be seen from Figure 20, the CFX SMI simulations show a higher back (negative axial velocity) flow compared to the CFX ISM, this is partly due to a higher pressure drop. The velocity profiles of CFX SMI simulations are virtually mesh independent at ≥ 49 M elements. The Polyflow profiles are less detailed than the CFX profiles, because of the difference in nodes across the gap of the screw flight. The Polyflow SMI profiles show a very similar velocity profile to the CFX SMI profile. Both CFX ISM and Polyflow ISM do not reach a mesh independent result. The Polyflow ISM profiles show the largest difference between the profiles. The ISM simulations show an asymmetric velocity profile, while a nearly symmetrical profile is expected. This asymmetry might disappear with further increase of the number of mesh cells. In general the velocity is quite low in al simulations and the gap between the flight and the barrel wall is small (<0.1 mm). Therefore, the influence of the flow in the gap is expected to be minor on the overall flow behavior in the

metering zone. With that in mind all the meshes show a reasonable result, except the coarsest meshes and the Polyflow ISM meshes. But the velocity profile between the barrel and the flight is more important with some specific screw geometries, such as a barrier screw and a Maddock mixer. In those cases, it is recommended to use Polyflow SMI, CFX SMI or CFX ISM and to determine the mesh dependency of the velocity profile in the barrel-flight.

Calculation time is dependent on mesh size, time step and the number of iterations needed to achieve convergence. The central processing unit (CPU) time per timestep is determined for each simulation technique and mesh. A calculation time needed for a second transient simulation is determined by extrapolating the CPU time. This extrapolation is based on a computer with 16 cores. Time consuming processes such as loading, partitioning, saving, etc. are not included in this calculation duration analyses.

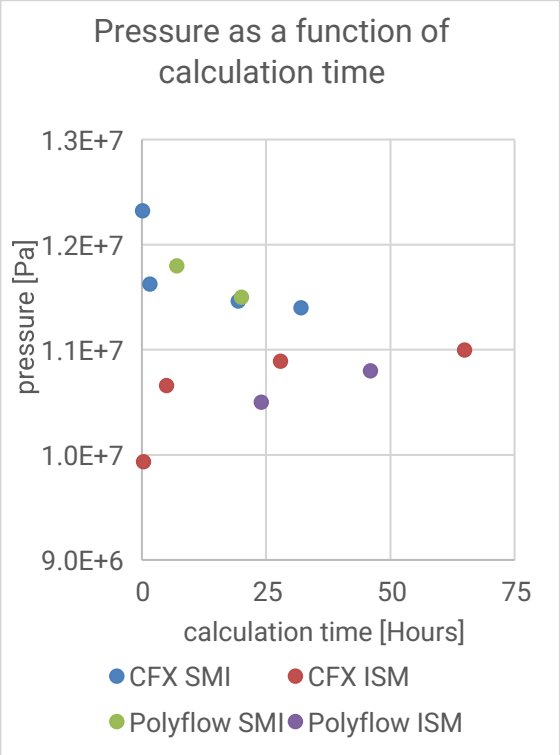

Figure 21. Pressure as a function of calculation time per second of transient simulation with a 16 core computer.

For transient CFX SMI 49 M simulation 19 hours calculation are needed per second and for transient CFX ISM 80 M simulation 28 hours per second. For a transient Polyflow SMI 0.78 M simulation 20 hours per second and for transient Polyflow ISM 0.69 M simulation.
40 hours per second are needed.

3.2.3 Conclusion and recommendations

Conclusions:

The difference in pressure drop between CFX SMI, CFX ISM, Polyflow SMI and Polyflow ISM are relatively small. With a high number of mesh cells, the difference in pressure drop between all 4 methods reduces to a maximum of 6.3 %.

A mesh of 49 M cells for CFX SMI and 80 M cells for CFX ISM were needed to achieve results with relatively little mesh cells size dependency. Meshing for ISM is a less time consuming than for SMI since the meshes are less complex. Furthermore, in ISM only the immersed solid (screw) needs remeshing with a change of screw. As a result, ISM has an advantage in comparing different screws.

In contrast, using SMI a change of screw geometry requires remeshing of most of the fluid domain, which is very time consuming.

The flow between screw flight and barrel can be simulated, but this requires large meshes and high computation costs and thus calculation time. With a standard screw geometry the influence of the flow on the whole extruder is low due to the small flight-barrel gap and the low local velocity.

For mixing purposes, 19 hours calculation are needed per second of transient CFX SMI 49 M simulation, 28 hours per second of transient CFX ISM 80 M simulation, 20 hours per second of transient Polyflow SMI 0.78 M simulation and 40 hours per second of transient Polyflow ISM 0.69 M simulation.

Recommendation:

It is recommended to use CFX for simulations using a Maddock screw since the flow profiles at the screw flight are more detailed with this software program.

It is further recommended to use the immersed solid method for extrusion simulations, since complex bodies and movement can be accurately simulated and computational costs and working hours are less compared to SMI. Disadvantage are the large meshes needed and with that high computational costs and the very long calculation time.

4 Experiments

The goal of the study in this document is to develop a procedure for simulating mix quality as an alternative to mix experiments. The material parameters were determined with a capillary rheometer as shown in section 4.1. The extruder and screw geometry are shown in section 4.2. This section also shows extrusion experiments to determine the extrusion temperature, pressure and flow rate.

4.1 Capillary measurements of HDPE to obtain a power-law function

Capillary rheometer measurements with HDPE were performed to determine an appropriate fluid model for the simulations. The rheological measurements and analyses were performed by the Professorship. The capillary rheometer and the HDPE were provided by Wavin T&I.

4.1.1 Theory

With a capillary rheometer the pressure (P) is measured, the capillary length (L), radius (R) and flow rate (Q) are imposed. With these parameters the relation between shear stress and the shear rate of the fluid can be determined. This section shows a method of using these parameters to determine the relation between shear stress (τ) and the shear rate ($\dot{\gamma}$) of the fluid. The wall shear stress (τ_w) inside the capillary can be described by:

$$\tau_w = \frac{\Delta P}{\Delta L}\frac{R}{2} \qquad 3$$

The shear rate at the wall (γ_w) can be described by the Weissenberg-Rabinowitsch equation [1]:

$$\dot{\gamma}_w = -\frac{Q}{\pi R^3}\left(3 + \frac{d\ln(Q)}{d\ln(\tau_w)}\right) \qquad 4$$

The relation between the wall shear stress and the flow rate is:

$$\ln(\tau_w) = a\ln(Q) + \ln(b) \qquad 5$$

The parameters a and b are constants when the temperature is constant. Equation 5 can be rewritten to:

$$\tau_w = bQ^a \qquad 6$$

Combining equations 4 and 5 results in:

$$\dot{\gamma}_w = -\frac{Q}{\pi R^3}\left(3+\frac{1}{a}\right) \quad 7$$

That can be rewritten to:

$$Q = \frac{-\pi R^3 a}{3a+1}\dot{\gamma}_w \quad 8$$

Combining equations 6 and 8 result in:

$$\tau_w = b\left(\frac{-\pi a R^3}{3a+1}\right)^a \dot{\gamma}_w^a \quad 9$$

This is similar to the power law:

$$\tau = m\dot{\gamma}^n \quad 10$$

Parameters *m* and *n* can be determined with:

$$m = b\left(\frac{-\pi a R^3}{3a+1}\right)^a \quad 11$$

$$n = a \quad 12$$

4.1.2 Measurement setup

Measurements were performed with the capillary rheometer of Wavin. All capillaries had a diameter of 2 mm. To correct for the in- and outflow effects, three different capillary were used: 5 mm, 10 mm and 20 mm. The rheological properties were measured at 200 °C and 220 °C. Most measurements were performed twice. All capillaries had smooth surfaces, except for a capillary of 20 mm long with an internal thread as its surface, which was used to determine whether a significant amount of wall slip is present.

4.1.3 Material

Measurements were performed using Marlex TRB-432 Polyethylene manufactured by Chevron Phillips Chemical Company [51]. This HDPE is an ethylene-hexene copolymer with good mechanical properties and a PE4710 rating for pipe applications. This is a bimodal HDPE, produced in multiple reactors and therefore having a broad molecular weight distribution, see Figure 22.

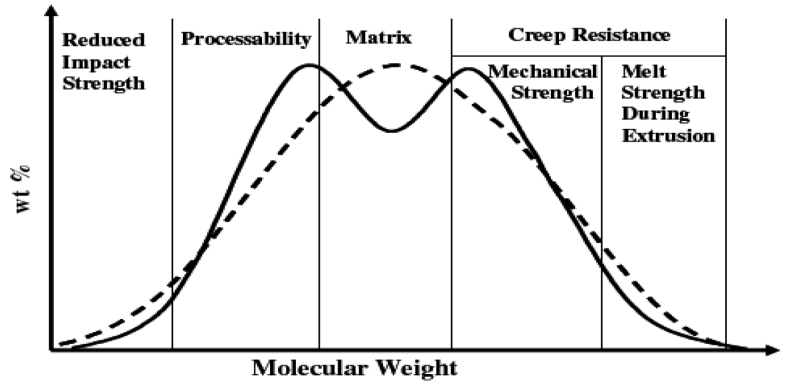

Figure 22. Schematic representation of molecular weight distribution of unimodal (- - -) and bimodal (----) PE. Figure copied from figure 2.5 of reference [52].

Low molecular weight material improve processability and high molecular weight material improve mechanical strength [53].

4.1.4 Results and observations

This section shows the measured pressure as a function of flow rate, temperature and capillary length. All results shown are an average of the measurements at one specific temperature, using one specific capillary and at one specific flow rate. The standard deviations are not shown in the results and are calculated to be on average 1% and at maximum 6%.

4.1.4.1 Instabilities and wall slip

Wall slip is often an interfacial phenomenon. Therefore, changing the fluid-wall interface will also change the slip behavior. Measurements were performed with a smooth 20 mm long capillary and with a 20 mm capillary with an internal thread (female) as a surface, see Figure 23.

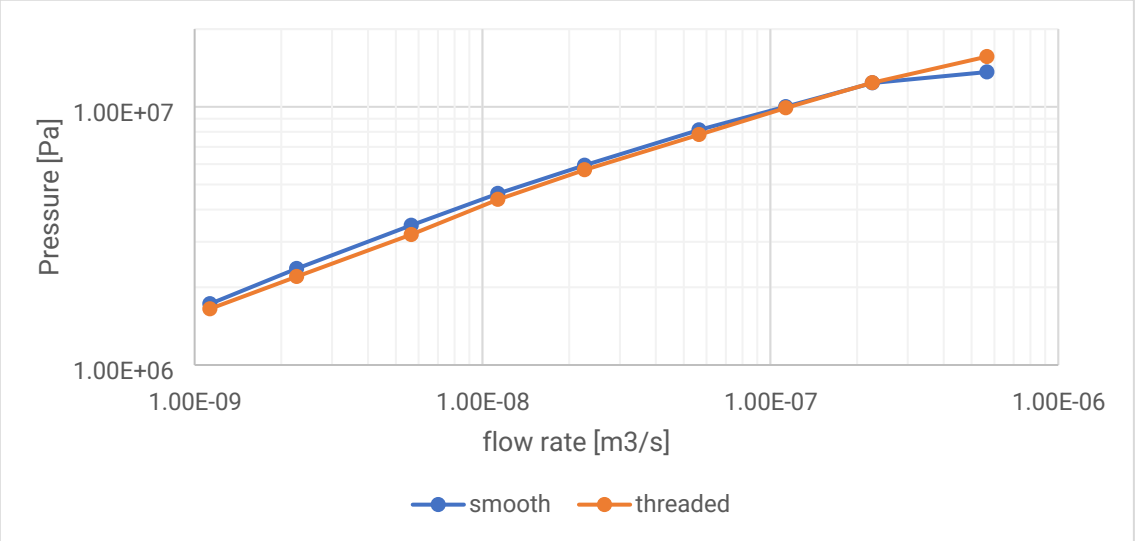

Figure 23. pressure as function of flow rate at 200 °C with a smooth capillary of 20 mm and a threaded capillary of 20 mm.

There is no discernable difference between the two measurements up to a flow rate of $2 \cdot 10^{-7}$ m^3/s. This suggests a very low slip velocity or no slip at all. At $6 \cdot 10^{-7}$ m^3/s the pressure drop with the threaded capillary is higher than the smooth capillary. This difference may very well be due to slip.

Most experiments with the smooth capillaries appeared instable at $2 \cdot 10^{-7}$ m^3/s. The pressure started to oscillate and the produced extrudate was not smooth. At higher flow rates the pressure is not stable with any of the measurements.

4.1.4.2 Bagley correction

$\Delta P/\Delta L$ is expected to be constant at a constant flow rate and a constant temperature. The measurements show a linear relation between P and L, see Figure 24.

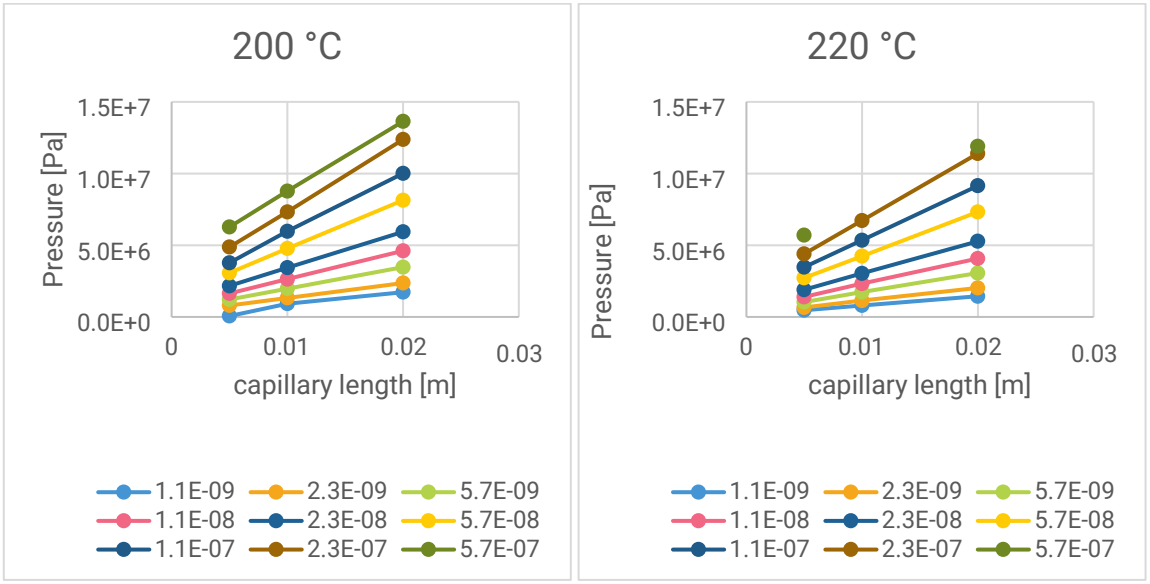

Figure 24. pressure as function of capillary length at various flow rates (in m^3/s). Left: measurements at 200 °C. Right: measurements at 220 °C. Note: the legend show the flow rate in m^3/s.

Pressure drops at the capillary inflow and possibly at the capillary outflow are expected, the Bagley correction is a method to take the effects of the inflow and outflow pressure drop into account. A Bagley correction of >0 m could be determined for all flow rates and temperature except the lowest flow rate ($1.1 \cdot 10^{-9}$ m^3/s) at 200 °C. This is most likely due to a measurement error at low pressures. Therefore, the measurements at $1.1 \cdot 10^{-9}$ m^3/s were not used for fitting the power law parameters.

4.1.4.3 Temperature dependence and shear thinning behavior

Wall shear stress, $\frac{d\ln(Q)}{d\ln(\tau_w)}$ and the wall shear rate were calculated. Wall shear stress as a function of wall shear rate is shown in Figure 25.

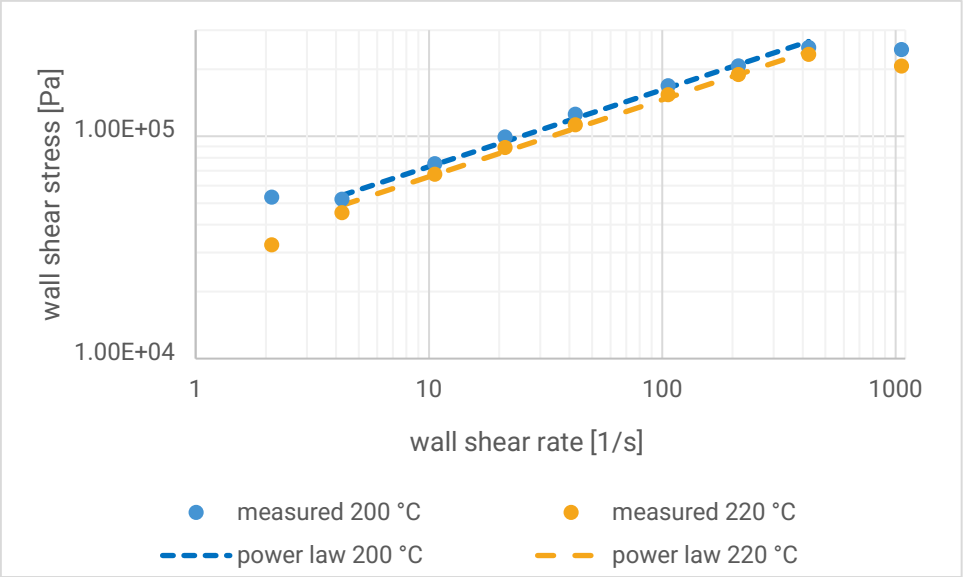

Figure 25. wall shear stress as function of wall shear rate at 200 °C and 220 °C. Both measurements and a fitted power law are shown.

Figure 25 shows a power relation between the wall shear stress and the wall shear rate for the range of 4 s^{-1} up to 500 s^{-1}. The outcomes below 2 s^{-1} are not included due to an uncertainty in the pressure measurements. The power relation between shear stress and flow rate breaks down at a shear rate of 1000 s^{-1}. This is most likely due to wall slip, see paragraph 4.1.4.1. A small reduction of the wall shear stress can be observed at 220 °C. The same power *n* was used for both temperatures, *n*=0.346. The material function (*m)* is different, $m = 3.29 \cdot 10^4$ Pa·s^{-n} at 200 °C and $2.97 \cdot 10^4$ Pa·s^{-n} at 220 °C. The fitted power law is shown in Figure 25.

4.1.5 Conclusion

Capillary rheology measurements were performed with HDPE at 200 °C and 220 °C. The HDPE was found to be shear thinning between a shear rate of 4 s^{-1} up to 500 s^{-1}. The fitted power law parameters are *n*=0.346, $m = 3.29 \cdot 10^4$ Pa·s^{-n} at 200 °C and $2.97 \cdot 10^4$ Pa·s^{-n} at 220 °C. This power law, or similar shear thinning model (such as a Bird-Carreau model), can be used as a material property in the extrusion simulations. Because power law characteristics at 200 °C and 220 °C are similar, extrusion simulations in this temperature range can be performed with isothermal conditions.

A comparison between rheological measurements with a smooth and a threaded capillary were in agreement at a wall shear stress up to $2 \cdot 10^5$ Pa. With a further increase in flow rate the threaded capillary showed an increase in pressure, while the smooth capillary did not show an increase in pressure. This might be due to wall slip with the smooth capillary, but was not studied further. It is recommended to keep the wall shear stress below $2 \cdot 10^5$ Pa in the simulations.

4.2 Experiments with a spiral Maddock and a pin mixing element

The goal of this project is to predict mixing behavior of a single screw extruder with flow simulations. At Wavin T&I several extrusion experiments were performed to determine the correct process parameters. These parameters serve as input for the extrusion simulations as are shown in part 2: *Mixing quantification* [42]. The parameters are the flow rate, the temperature and the screw rotational velocity. This section (4.2) shows the extrusion experiments. The materials are reported in section 4.2.1. The measurement setup is shown in section 4.2.2. The results are shown in section 4.2.3. A conclusion and recommendation for this project are presented in section 4.2.4.

4.2.1 Geometry and Materials

The extrusion experiments were performed with a single screw extruder with a die for pipe extrusion. The 75 mm diameter screw has a feed section, a barrier section, a spiral Maddock mixer and a pin mixer.

Figure 26. 75 mm diameter extruder screw with a barrier section, a spiral Maddock mixer and a pin mixer.

Pressure and melt temperature are measured in de barrel between the extruder and the die. The barrel is divided into several temperature zones and is managed by the extruder computer. The mass flow rate is set in the extruder computer, the computer manages the screw rotational velocity and mass flow rate of the feeder.

The extrusion material was HDPE (Marlex TRB-432, Chevron Phillips Chemical Company). The HDPE was rheologically characterized at 200 °C and 220 °C with a capillary rheometer, see section 3.1.

4.2.2 Experimental setup

Extrusion experiments were performed at incrementally increasing mass flow rates. The temperature was set to 200 °C in every barrel temperature zone. The extruder computer registered the melt temperature, the pressure, the flow rate, the percentage of the maximum torque and the screw rotational velocity.

Specific energy (SE) was calculated with the rated maximum power of the extruder motor (P_{rated} = 185 kW), the percentage of the maximum torque ($T_{relative}$), the rotational velocity of the screw (ω) and the rated maximum rotational velocity (ω_{rated} = 182 rpm).

$$SE = \frac{P_{rated} T_{relative} \dfrac{\omega}{\omega_{rated}}}{\text{flow rate}} \qquad 13$$

4.2.3 Results

Extrusion experiments were performed during 2.5 hours, after an increase in flow rate at least 390 s were needed for the system to stabilize. The average measured values are shown in Figure 27.

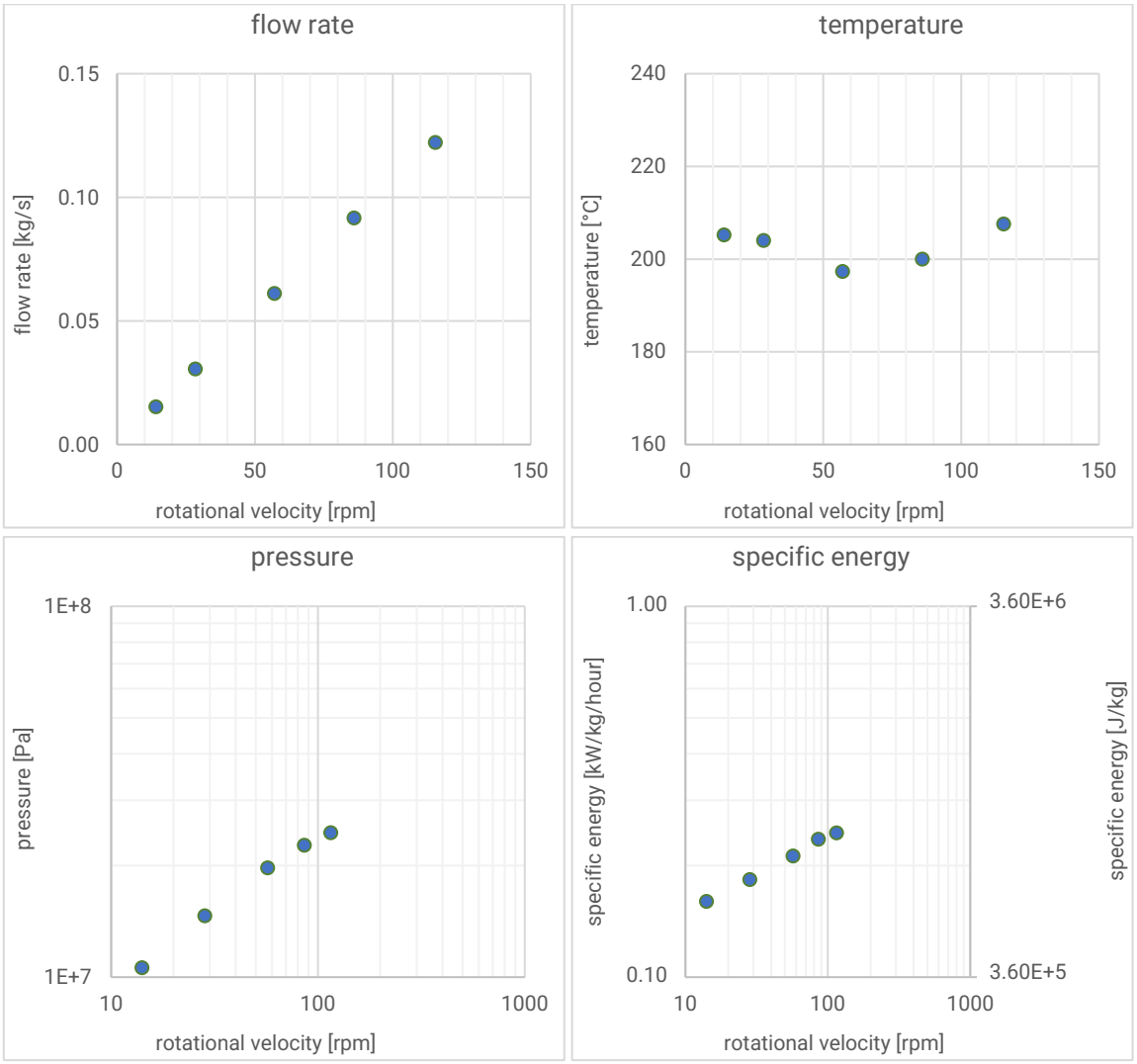

Figure 27. Flow rate, melt temperature, pressure and specific energy as a function of screw rotational velocity. Note: the flow rate and temperature graphs have linear axis, both the horizontal and vertical axis of the pressure and specific energy graphs are on a logarithmic scale.

The pressure is a power function of the flow rate, which is in agreement with the power law determined with the capillary rheology. A transition from stick to wall slip was not observed since the measured flow rate is a linear function of the screw velocity and the pressure is a power function of the flow rate. The melt temperature is near the barrel temperature (200 °C) and differs somewhat per rotational velocity. The temperature dependency of the viscosity of the HDPE is minor in the range of 200 °C to 220 °C, therefore the temperature differences have a minor influence on the measured values.

4.2.4 Conclusion and recommendations

Extrusion experiments were performed at several flow rates. The screw rotational velocity, flow rate and temperature settings can be used as input parameters in the extrusion simulations in part 2: Mixing quantification [42]. Slip was not observed, therefore a no-slip condition in the simulations is recommended. Furthermore, the measurements show a low temperature gradient in the extruder. The temperature dependency of the HDPE is minor in the range of 200 °C to 220 °C. The low thermal dependency and the low temperature gradient results in a low viscosity gradient due to temperature.
Based on the experimental results, it can be concluded that the assumption of isothermal flow simulation is justified for the used material. Thus it is recommended to neglect temperature dependency on viscosity in the numerical simulations. Also, the processing parameters found in the experiments are suitable as settings for the simulations.

5 Simulations

The single screw extruder used for the experiments (see section 4.2) consists of two mixing sections: a spiral Maddock and a pin mixer. One mixing section is specifically designed for dispersive mixing and the other for distributive mixing. This chapter is focused on finding optimal simulation settings for both the spiral Maddock and the pin mixer. Both these mixing section were simulated separately to find the optimal settings with respect to grid-structure and grid-independency, see sections 5.1 and 5.2.

5.1 Spiral Maddock simulations

This section is focused on finding a suitable mesh for the spiral Maddock simulation. Simulations with different meshes were evaluated by comparing the pressure and velocity inside the spiral Maddock element. Extra attention is given to the shear rate which is associated with dispersive mixing quality.

5.1.1 A mesh study for spiral Maddock simulation

Predicting mixing behavior of a single screw extruder with flow simulation is the goal of the sustainable extrusion project. Extrusion experiments were performed with a single screw extruder, see section 4.2. The screw consists of several sections including a spiral Maddock. Fluids flowing through this section are subjected to very high shear stress. Therefore, the Maddock mixer is a good dispersive mixer. An objective of this project is to model the mixing behavior of the spiral Maddock. Therefore, a CFD simulation of the spiral Maddock is needed and particle tracking to determine the mixing behavior.

This section is focused on finding a suitable mesh for the spiral Maddock simulation. The pressure and velocity inside the spiral Maddock will be compared in simulations with different meshes.

5.1.1.1 Simulation setup

The simulations were performed with the immersed solid method (ISM) in Ansys CFX. The setup is reported in this paragraph.

5.1.1.1.1 Used hardware

The simulations were performed sequentially with a cluster of three HP computers (type Z820) with the following specifications:

Windows 10, 64-bit
2X Intel Xeon CPU E5-2680, 2.7 GHz
256 Gb ram, 1600 MHz

In total 48 cores and near 768 GB RAM was available for each simulation.

5.1.1.1.2 Extruder setup and geometry simulation setup

To construct a CAD model of the screw, it is necessary to determine its geometry. The barrel diameter is 0.0375m. The spiral Maddock is comparable to a barrier screw as they both use a barrier flight. The spiral Maddock consist of three inflow channels and three outflow channels, see Figure 28.

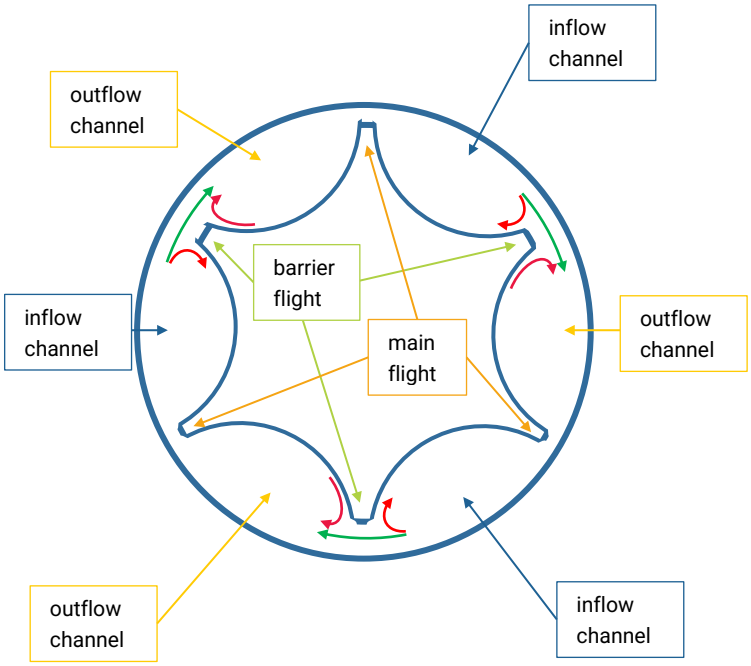

Figure 28. Schematic cross section of a spiral Maddock.

The inflow and outflow channels are connected via a 0.6 mm gap between the barrel and the barrier flight. All fluids flowing into the inflow channels, must cross the barrier flight in order to enter the outflow channel to exit the spiral Maddock. The flow in the gap, between the barrier flight and the barrel wall, consist of a pressure flow and a simple shear flow, see Figure 29.

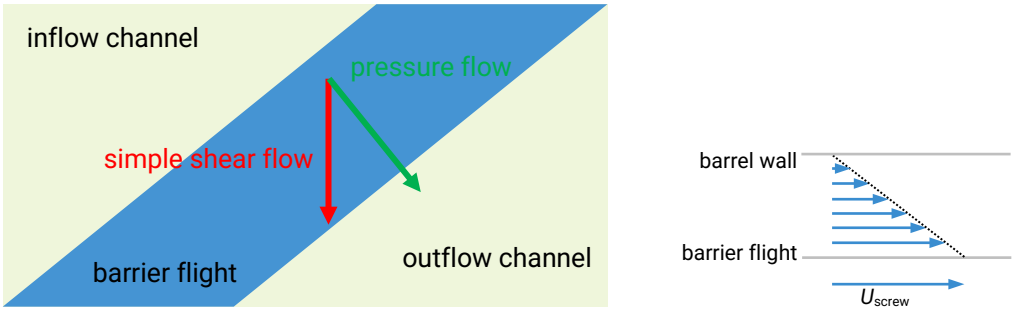

Figure 29. Schematic illustration of flow across the gap between the barrier flight and the barrel. Left: a top view of the barrier flight. Right: representation of simple shear velocity field in the gap between the barrier flight and the barrel.

The simple shear flow, in the gap, is due to the rotation of the barrel. The shear stress is very high in this simple shear flow and promotes dispersive mixing. The velocity profile is represented by two components, the angular velocity profile and an axial velocity profile. The angular velocity is mainly due to rotation of the barrel (simple shear flow) and some pressure flow, the axial velocity is mainly due to pressure flow.

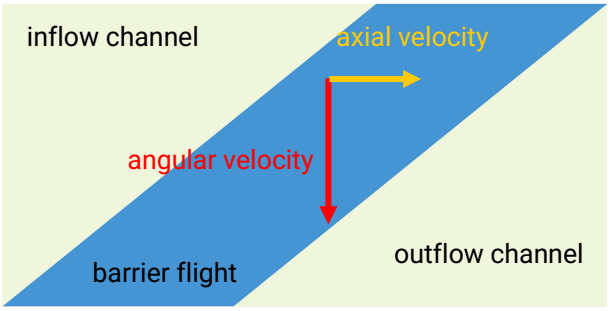

Figure 30. Angular velocity and axial velocity in the gap between the barrier screw and the barrel wall.

The velocity profile, in the gap, should be mesh independent for reliable mixing behavior.

5.1.1.1.3 Boundary conditions

The boundary conditions are similar to the extrusion settings during the extrusion experiments at the lowest flow rate, see section 4.2. The mass flow rate was set to 0.015 kg/s, see Figure 31. A 0 Pa condition was set at the outflow opening. During the experiments the screw rotates with 14 rpm and the barrel is stationary. This is in contrast with the simulations where the screw is stationary and the barrel wall rotates with 14 rpm. No wall-slip was included in the simulation, the velocity of the fluid at the wall is equal to the velocity of the wall.

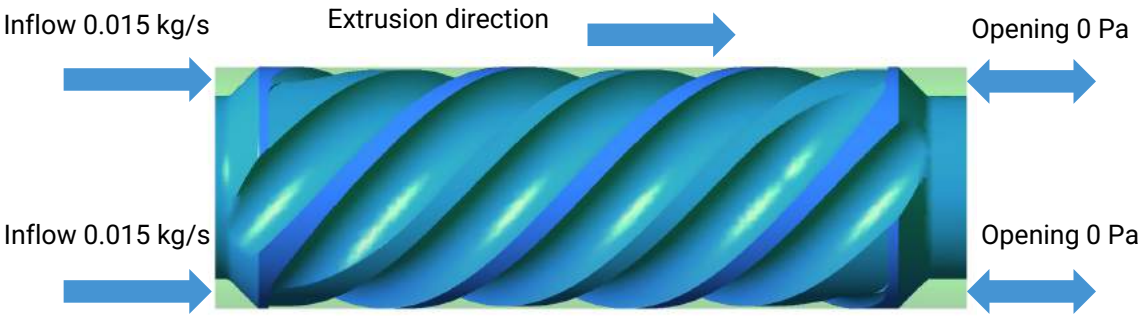

Figure 31. Side view of the spiral Maddock CAD. The screw is in blue, the fluid in green. Note: flow in the simulations is from left to right.

The gap between the main flight and the barrel is very narrow (0.06 mm) to prevent fluids to flow through.

Preliminary spiral Maddock simulations showed an instability which originated in this narrow gap. This instability is probably due to the relative few mesh cells in the gap. To prevent this instability the main flight was extended beyond the barrel wall. With this setup the gap between the main flight and the barrel wall does not exist in the simulations. The influence of this simplification is expected to be minor since simulations of a metering zone showed that the influence of the flow between the flight and the barrel is minor, see section 3.2.2.

5.1.1.1.4 Material parameters

Extrusion experiments were performed with HDPE grade Marlex TRB-432 (Chevron Phillips Chemical Company, see section 4.2). The viscosity as function of shear rate was determined with a capillary rheometer, see section 4.1. Measurements were performed in a shear rate range from $\dot{\gamma} = 4\ s^{-1}$ up to $\dot{\gamma} = 500\ s^{-1}$ at 200 °C. A power law was fitted onto the rheological measurements with n=0.346 and m=3.29·10^4 Pa·s^{-n}.

A power law gives infinite viscosity at zero shear rate leading to numerical instabilities. Therefor a Bird-Carreau model was used in the simulations:

$$\eta = \eta_\infty + (\eta_0 - \eta_\infty)\left(1+(\lambda\dot{\gamma})^2\right)^{\frac{n-1}{2}} \qquad 14$$

The viscosity at infinite shear rate (η_∞) is 1 Pa·s, the viscosity at zero shear rate (η_0) is 3.01184 MPa·s. The relaxation time (λ) is 1000 s. The Bird-Carreau and the power law are almost identical in the shear rate range of $\lambda^{-1} > \dot{\gamma} > \left(\frac{\eta_\infty}{m}\right)^{\frac{1}{n-1}}$. λ and η_∞ are chosen in such a way that the power law and the Bird-Carreau model show similar behavior at $10^{-3} > \dot{\gamma} > 8 \cdot 10^{6}$. This range seems reasonable since lower and higher shear rate are not expected to have a significant influence on the simulation.

5.1.1.1.5 Mesh

A fluid domain and an immersed solid were created.

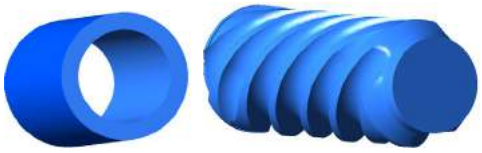

Figure 32. Left: fluid domain. Right: immersed solid domain.

The two domains were meshed separately.

One part of the fluid domain mesh consists of a structured mesh with cubical cells near the barrel wall see Figure 33. The height of this structured part is as large as the gap between the barrier flight and the barrel (0.6 mm). This ensures a minimum number of cells between the barrier flight and the barrel wall.

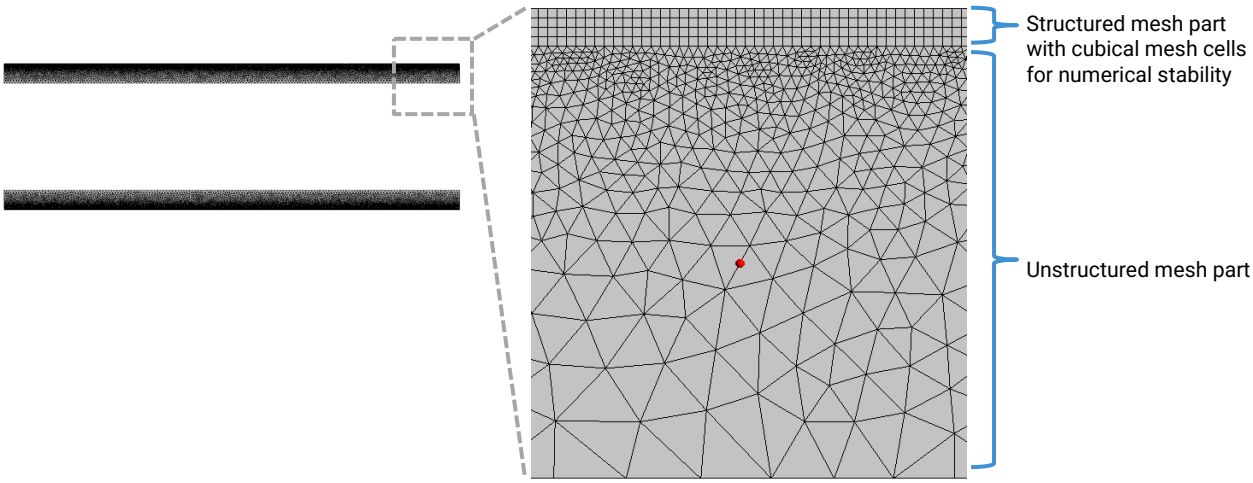

Figure 33. Cross section of a fluid domain mesh.

The rest of the fluid domain consists of an unstructured mesh. Several meshes were made in order to find the proper mesh density, see Table 3.

The number of cells between two walls often has a great impact on the simulation and is lowest between the barrel and the barrier flight. Therefore, the mesh between the barrier flight and the barrel is expected to have the most significant impact on the simulation.

Table 3. mesh sizes

Mesh name	Number of cells between the barrier flight and the barrel	Cubical cell size [mm]	Number of mesh cells of the complete fluid domain
4	4	0.150	58 M
6	6	0.100	109 M
8	8	0.075	207 M
10	10	0.060	302 M
12	12	0.050	479 M

Different meshes were made whilst keeping all settings the same, except for the cell size in the structured part. Of course a reduction in cubical cell size also results in an increase of cells in the unstructured part since these are connected.

The screw mesh in the immersed solid domain does not have a great impact on the computational costs. Therefore, a single fine mesh was made for the screw. This unstructured mesh was used in each simulation.

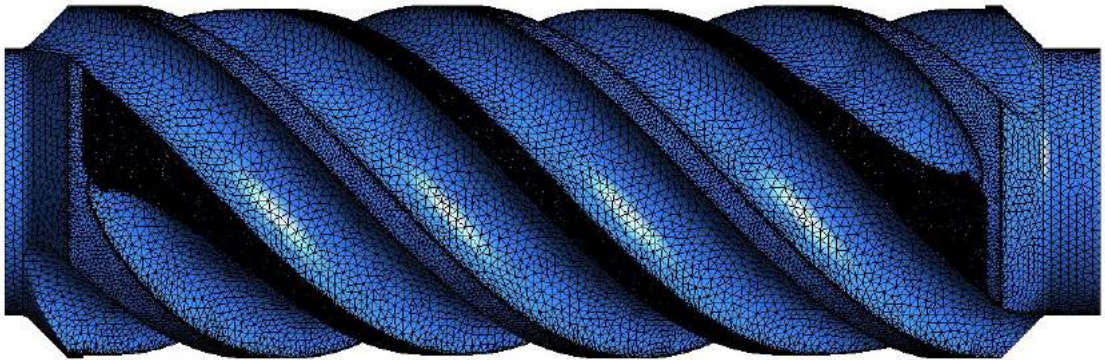

Figure 34. Side view of the immersed solid domain mesh / screw mesh.

It is preferred to have a well-defined gap between the barrel and the barrier flight. The fluid domain mesh is very fine in this area, the barrier flight also has a very fine mesh.

5.1.2 Results

The results with the different meshes are shown in this section.

5.1.2.1 Computational costs

The Ansys CFX reserves an amount of RAM for a simulation, Table 4 shows the RAM per mesh.

Table 4. computational costs

Mesh name	Number of cores used per simulation	RAM requirements
4	48 (3x16)	140 GB
6	48 (3x16)	216 GB
8	48 (3x16)	343 GB
10	48 (3x16)	497 GB
12	24 (3x8)	710 GB

Due to RAM limitations the simulation with mesh 12 was performed with 24 (3x8) threads. All other simulations were performed with 48 (3x16) threads. The memory requirements of simulations 4 and 6 were < 256 GB, therefore could have been solved on a single Z820. The memory requirements were > 256 GB for simulations 8, 10 and 12, therefore they could only be solved with a cluster of several Z820 computers.

5.1.2.2 Pressure inside the spiral Maddock

The pressure inside the extruder is shown in Figure 35.

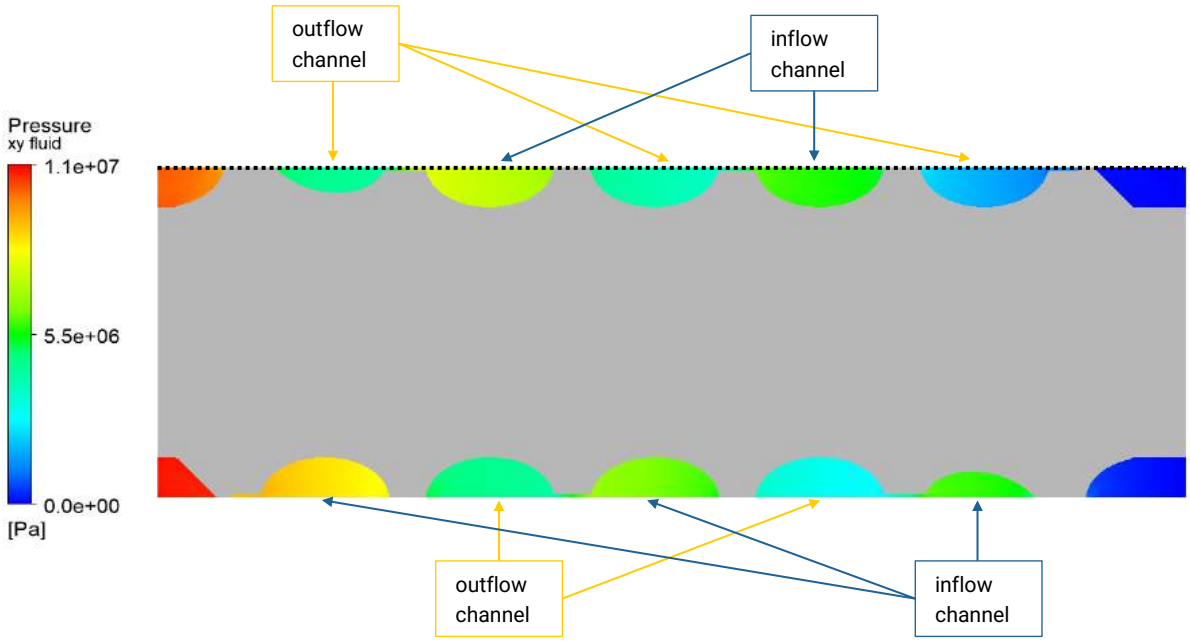

Figure 35. Pressure in a cross section of the spiral Maddock. Note: flow is from left to right.

Because in the spiral Maddock pressure is required to force a fluid over the barrier flight, the pressure at the inflow is higher compared to the one in the outflow channel next to it. The pressure at the top of the spiral Maddock, as marked by a black dotted line in Figure 35. The pressure, along the dotted line, is plotted as a function of axial distance (Figure 36) in order to compare the pressure simulated with different meshes.

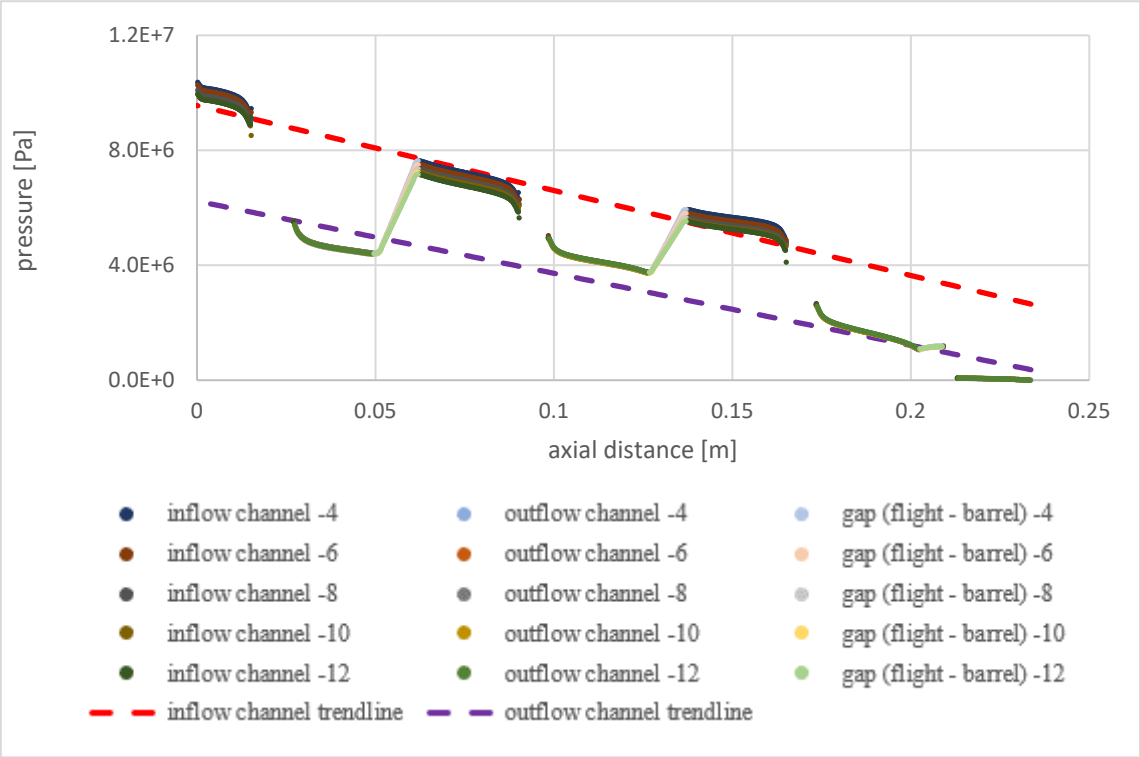

Figure 36. Pressure in the spiral Maddock as a function of axial distance. There is a lot of overlap between the various simulations leading to overlapping datapoints. Note: the direction of axial flow is from left to right in this graph.

For every mesh size the simulations show a very similar pressure inside the spiral Maddock. In Figure 36 4 areas can be distinguished:

- Inflow channel (areas corresponding to the red trendline)
- Outflow channel (areas corresponding to the purple trendline)
- The gap between the barrier flight and the barrel (the only regions with an increase in pressure ($0 < dp/dz$)
- Inside the screw (positions without data points)

No pressure is shown in Figure 36 where the line cuts the screw. The fluid flows from the inflow channel to the outflow channel in a direction opposite to the extrusion direction. Figure 36 shows a positive dP/dz inside the gap, while it is negative for all other areas in the extruder. Trendlines of the pressure in the inflow and outflow channels are shown Figure 36. These trendlines show a linear relation between the pressure and axial distance (dp/dz = constant). The difference in pressure between the inflow and outflow channel trendlines ranges from 2 MPa up to 3 MPa.

The difference in pressure between the simulations is small with respect to the total pressure difference of 11 MPa. The maximum difference in pressure in the inflow channels is 0.9 MPa between the simulations. The maximum difference in both the gap and the outflow channels is 0.5 MPa. All the simulations are in agreement with each other, therefore the coarsest mesh (4) is suitable for simulating the pressure drop in the spiral Maddock.

5.1.2.3 Velocity between the barrier flight and the barrel

Dispersive mixing is expected to happen mostly in the gap between the barrier flight and the barrel. Therefore, mesh independent behavior of the simulation is relevant in this gap. The flow in the gap consists of a pressure flow and a simple shear flow, see paragraph 4.2.1.1.2. Velocity as function of radial distance was studied in the gap. Figure 37 shows a line in the gap where the velocity was determined.

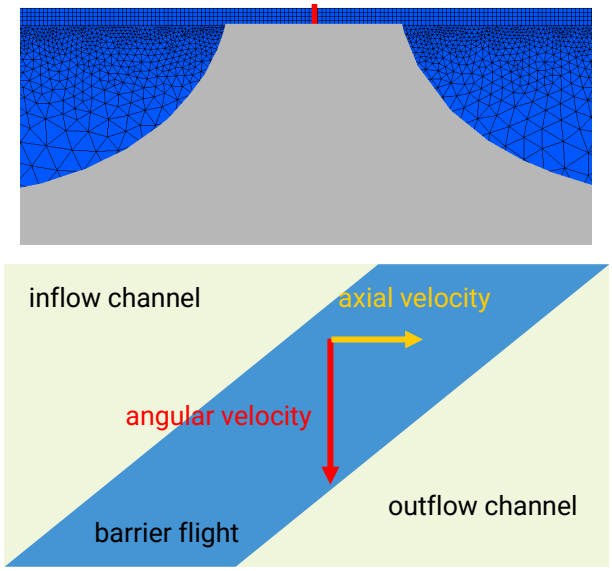

Figure 37. Top: radial line (red) where the velocity was determined between the barrier flight (grey) and the barrel (white). Bottom: angular velocity and axial velocity in the gap between the barrier screw and the barrel wall.

Both the axial velocity and the axial shear rate, in the gap, as function of radial distance are shown in Figure 38.

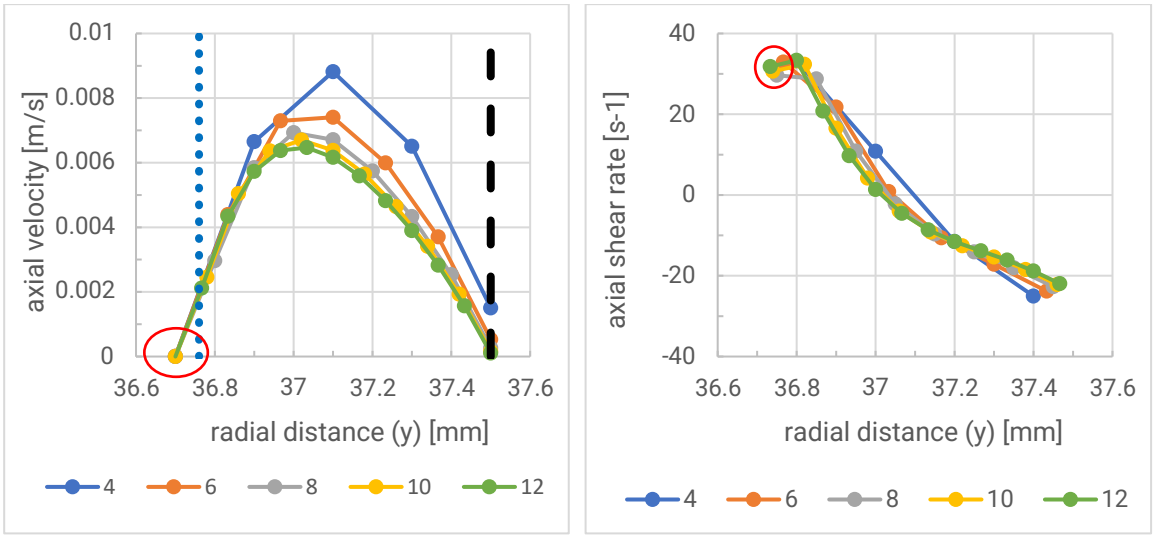

Figure 38. Left: axial velocity between the barrier flight and the barrel as function of radial distance (y). The position of the barrier flight is marked with a blue dotted line, the position of the barrel is marked with a black striped line. Right: axial shear rate as function of radial distance.

The position of the screw in the CAD is marked with a blue dotted line. The velocity is not zero at the screw wall, but at the nearest mesh node inside the screw wall. This is due to the use of the immersed solid method to describe the interface between the immersed solid domain and the fluid domain. The exact position of the interface depends on the meshes of both the immersed

solid domain and the fluid domain and can therefore not be imposed to be exactly at the screw wall. This is in contrast to the zero wall velocity at barrel wall where there is not an immersed boundary.

The velocity and shear rate near the screw wall shows an improbable behavior, see Figure 38 marked by a red circle. This behavior has probably a numerical origin in the immersed solid method. The axial velocity is low is this region, therefore an error in the velocity field will have a minor impact on the results.

The simulation with the coarse meshes show a small amount of velocity at the barrel wall, this is not in agreement with the zero wall velocity boundary condition. It is not known what the origin is of this discrepancy but it disappears when using the larger meshes.

The axial velocity profile is similar to a pressure flow, although there is some difference as evident by the shear rate as function of radial distance. A pure pressure flow shows a linear relation between the shear rate and the radial distance, whereas a slight curvature is visible in Figure 38.

The axial velocity field between the barrier flight and barrel reduces somewhat with increasing mesh density. There is almost no difference between mesh 8, 10 and 12. The difference in velocity between the simulations is negligible, therefore the coarsest mesh (4) is suitable for simulating the spiral Maddock.

Dispersive mixing, in the spiral Maddock, is mainly due to the high shear stress between the barrier flight and the barrel wall. Therefore mesh independent modeling of dispersive mix quality requires mesh independent modeling of shear rate between the barrier flight and the barrel wall. Both angular velocity and angular shear rate, in the gap, as function of radial distance are shown in Figure 39.

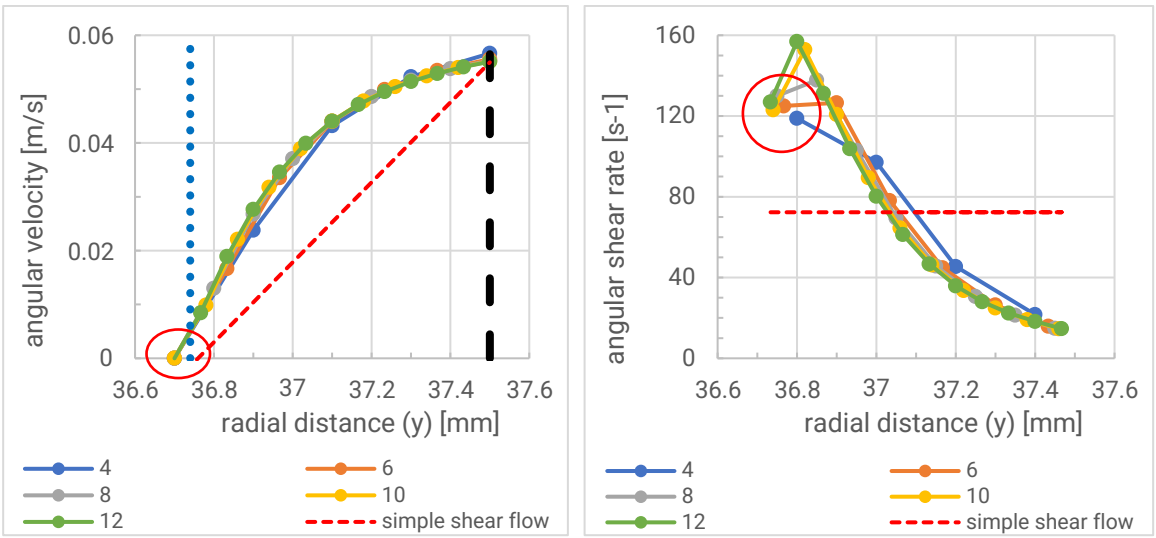

Figure 39. Left: angular velocity between the barrier flight and the barrel as function of radial distance (y). The position of the barrier flight is marked with a blue dotted line, the position of the barrel is marked with a black striped line. Right: angular shear rate as function of radial distance.

The angular velocity and shear rate profiles show an improbable behavior near the screw wall (marked with a red circle in the above figure). This is similar to the behavior of the axial velocity near the screw wall. The simulated velocity is low is this region, therefore an error in the velocity field will have a minor impact on the results.

The velocity between the barrier flight and the barrel wall has a simple shear component and a pressure component, see 5.1.1.1.2. The velocity profile and the shear rate of a pure simple shear flow was calculated analytically and is shown in the above figure (red dotted line) as well. The angular velocity profile shows some curvature. A pure simple shear flow would show a linear relation between velocity and radial distance. The curvature is due to the pressure flow component. The difference between a pure simple shear flow and the angular flow in the gap is even more pronounced in the difference in shear rate. Like the axial velocity, the angular velocity field between the barrier flight and barrel changes somewhat with increasing mesh density. Again, there is almost no difference between mesh 6, 8, 10 and 12. The difference in velocity between the simulations is negligible, therefore the coarsest mesh (4) is suitable for simulating the spiral Maddock.

5.1.3 Conclusion and recommendations

Simulations with 5 different meshes were performed. The computational costs increase rapidly with increasing mesh size. The pressure inside the extruder shows minor differences between simulations. Therefore, the coarsest mesh (4) is suitable to simulate the pressure drop inside the spiral Maddock.

The differences in velocity between the barrier flight and the barrel, between the various simulations are small. The velocity fields of mesh 8, 10 and 12 show almost no difference. The simulation with mesh 4 shows some difference in the simulations with finer meshes although the differences are small.

Due to the low computational costs of mesh 4, this mesh is considered useful for simulating several different setups and geometries and when post processing all these different simulation setups. Therefore, the coarsest mesh (4) is recommended for simulating the spiral Maddock.

5.2 Pin mixer simulations

Extrusion experiments were performed with a single screw extruder. The results are reported in section 4.2. The screw consists of several sections including a pin mixer, which is known as a good distributive mixer. In this section, the pin mixer is simulated. This section is focused on finding a suitable mesh for the simulation of a pin mixer. Simulations with different meshes were evaluated by comparing the pressure and average viscosity inside the pin mixer.

5.2.1 Simulation setup

In this section the geometry of the pin mixer, the boundary conditions and mesh parameters are described.

5.2.1.1 Geometry

The screw and barrel geometry were measured and a CAD model was made of the screw of the pilot extruder from Wavin. The barrel diameter is 0.075 m. The pin mixer consists of three inflow channels and one outflow channel. The inflow channels of the pin mixer are the outflow channels of the spiral Maddock, see section 5.1. The outflow channel of the pin mixer is at the end of the extruder screw. In front of the inflow channels and at the end of the outflow channel is some extra space (0.03m) for the development of the flow in the simulation. The main flight was to ensure no gaps exist between the main flight and the barrel wall, as it was determined that even a narrow gap leads to a simulation instability (see also 5.1.1.1.3)

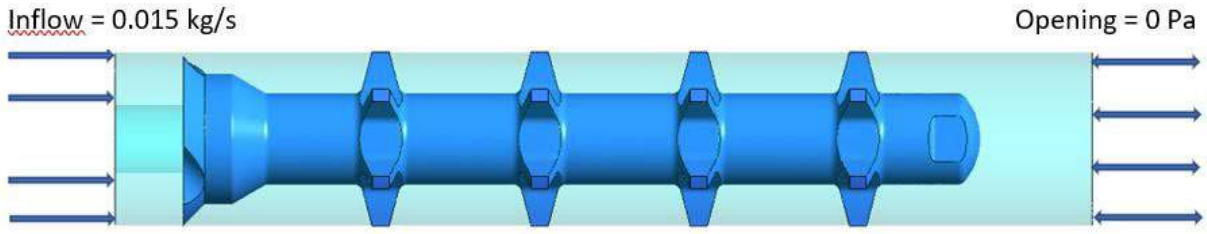

Figure 40. Side view of the pin mixer.

5.2.1.2 Boundary conditions and material parameters

The boundary conditions and material parameters are identical with the spiral Maddock simulation (paragraphs 5.1.1.1.3 and 5.1.1.1.4). In short: a mass flow rate condition was set to 0.015 kg/s. A 0 Pa condition was set at the outflow opening. The screw rotates with 14 rpm and the barrel is stationary. A zero wall velocity condition was set on the barrel wall. The Immersed Solid Method was used for rotating screw. The fluid model is a Bird-Carreau fluid, see equation 14, with n = 0.346, λ = 1000 s, η_0 = 3.01184 MPa·s and η_∞ = 1 Pa·s.

5.2.1.3 Mesh and mesh study parameters

For this study a fluid domain and an immersed solid are needed and were meshed separately. The fluid domain mesh consists of a mesh with fine unstructured tetrahedral cells. Structured cells were difficult to create because of the pins in the pin mixer. As a rule of thumb, a simulation with the correct mesh density does not change when the mesh cell density is increased.

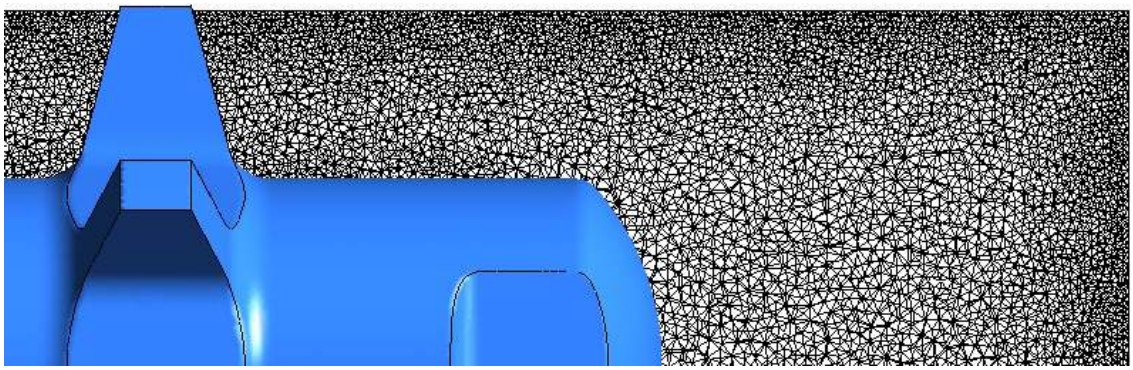

Figure 41. Cross Section of a mesh with a 0.75 mm element size.

To identify the proper mesh size and density, 4 different meshes varying element sizes were made. Element size was incrementally decreased from 1.25 mm down to 0.5 mm. Of course, a reduction in the element size also results in an increase of cells and an increase of the calculation time. In this study al other element properties (like aspect ratio) were kept constant.

The screw mesh size does not have a great impact on the computational costs. Therefore, a single fine mesh was made to represent the screw. This unstructured mesh was used in each simulation.

A mesh is dense enough when relevant parameters do not change (significantly) with an increase of mesh density. Mesh independent pressure difference over the pin mixer is an indicator of a good quality mesh. Furthermore, the velocity field is a very relevant parameter for distributive mixing. The average viscosity was used as a macroscopic parameter coupled with the velocity field. The viscosity of the fluid is a function of the velocity gradient, because it is a shear thinning material. Therefore, a mesh independent velocity field should show a mesh independent average viscosity.

5.2.2 Results

The pressure drop of the total pin mixer is about 29 bar in this simulation setup, including 10 bar at the transition from the extra space at the inflow and the beginning of the pin mixer. In reality, this free space doesn't exist, therefore the total pressure drop of the pin mixer will be about 19 bar. Both the pin mixer and the spiral Maddock consume pressure, but the spiral Maddock consumes far more with 110 bar compared to only 19 bar for the pin mixer.

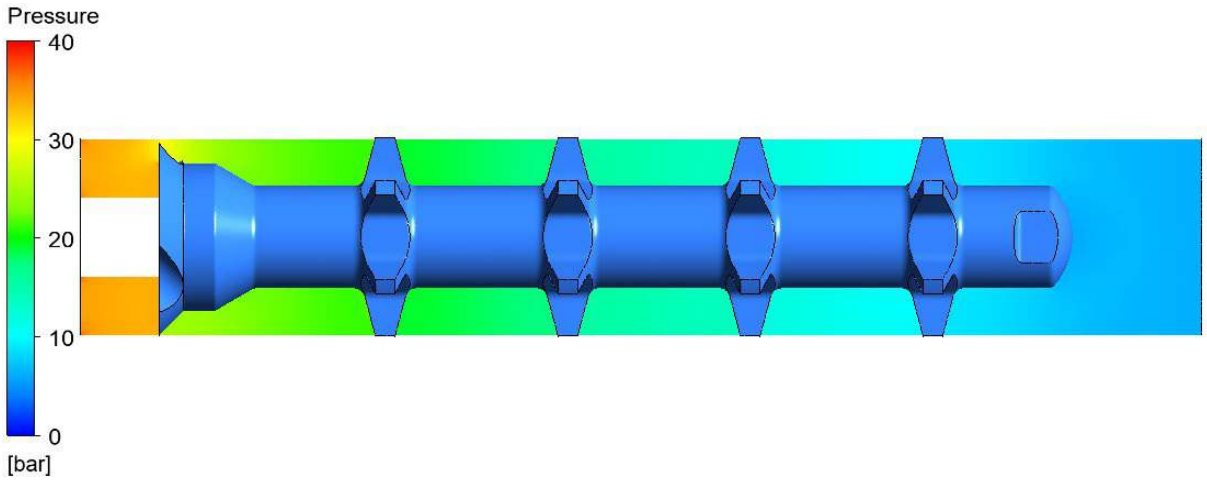

Figure 42. Total pressure drop of the pin mixer

The velocity of the fluid near the pin mixer is much higher than the velocity in the rest of the barrel (Figure 43). The rotation of the pin mixer also creates additional rotational velocity and therefore the velocity around the pin mixer is higher.

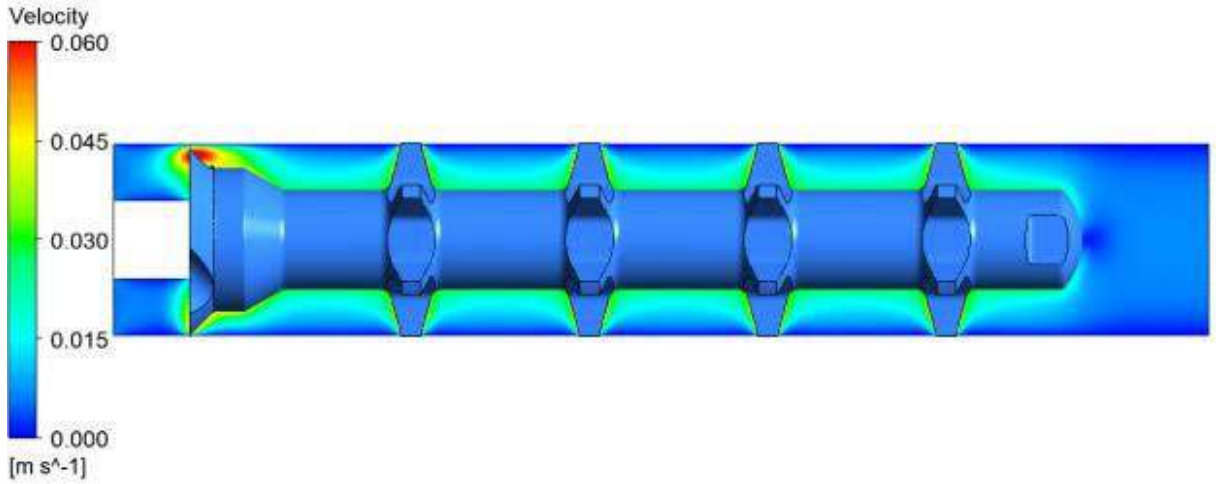

Figure 43. Velocity profile of the fluid at the pin mixer.

The velocity created by the rotation of the pin mixer is higher than the velocity created by the inflow (axial velocity). This is natural as the rotational velocity should be higher than the axial velocity to create a good quality of mixing.

In Table 4 the results of the simulations with different mesh sizes is shown.

Table 4. Mesh size, pressure and average viscosity.

Element size [mm]	Number of mesh cells	Pressure drop [bar]	Average dynamic viscosity [Pa.s]	Calculation time on 6 CPU cores [h]
1.25	8.88 M	28.9	85023	1
1	12.36 M	29	96867	2
0.75	22.19 M	29	108701	4
0.5	53.57 M	29.1	111012	17

An increase in element size beyond 0.75 mm shows that the average dynamic viscosity and pressure drop no longer change a lot, but the calculation time does change, see Table 4. Therefore, the element size of 0.75 mm is chosen to study the flow field in the pin mixer.

5.2.3 Conclusion

The simulation of the pin mixer has reliable results with at most an element size of 0.75 mm. These simulations can be calculated in about 4 hours with 6 CPU cores. Furthermore, the pin mixer consumes far less pressure (19 bar) compared to the spiral Maddock (110 bar).

6 Conclusion

Predicting mixing behavior of a single screw extruder with computational fluid dynamics (CFD) simulations is the goal of the sustainable extrusion project. The following research question was answered in this document:

What is a proper simulation method for polymer extrusion?

The finite element method (Ansys Polyflow) and finite volume method (Ansys CFX) were studied to answer the research question. Furthermore, the immersed solid method (ISM) and the sliding mesh interface (SMI) simulation techniques were studied. The programs and techniques were compared simulating the same single screw extruder. Large meshes (>10^7 cells) were needed for extruder simulation due to the important small details in the geometry like the gap between the barrier flight in the Maddock and the barrel wall. CFX is more suitable than Polyflow, in achieving mesh independent results with such large meshes. Similar results were found between CFX ISM and CFX SMI. ISM is applicable to more complex movement of bodies compared to SMI.

CFX ISM was selected as the preferred simulation technique for mixing behavior in single screw extrusion due to the above-mentioned advantages.

7 Recommendations

Sections of a single screw extruder were simulated such that mesh independent flow fields are obtained. These simulation can be used for determining the mixing quality. It is recommended to study methods to quantify mix quality with simulated flow fields as an input.

With the simulations only mixing sections of the extruder were included. However, the barrier screw does contribute to polymer mixing and it is therefore recommended to include the barrier screw and the melting process in the simulation procedure. Furthermore shear rate are high with some mixing elements, it is recommended to study the effect of viscous dissipation on the flow fields.

8 Acknowledgements

This study was financially supported by Tech For Future (TFF) and Wavin T&I. The study was conducted by Windesheim University Professorship for Polymer Engineering. Wavin T&I provided HDPE, a capillary rheometer for rheological measurements and a single screw extruder for extrusion experiments. Furthermore, Wavin T&I provided feedback on this study and knowledge of the extrusion process.

References

1. Tadmor, Z. and C.G. Gogos, *Principles of Polymer Processing*. 2006: Wiley.
2. Manas-Zloczower, I. and J.F. Agassant, *Mixing and Compounding of Polymers: Theory and Practice*. 2009: Hanser.
3. Kutz, M., *Applied plastics engineering handbook: processing and materials*. 2011: William Andrew.
4. Ogbobe, O., *Dispersion of additive masterbatches in polyolefin plastics*. 1985, © Okoro Ogbobe.
5. Rothon, R.N., *Fillers for Polymer Applications*. 2017, Springer Verlag.
6. *What is Carbon Black?* 2018; Available from: http://monolithmaterials.com/innovative-technology/what-is-carbon-black/.
7. Alemaskin, K., *Entropic Measures of Mixing in Application to Polymer Processing*. 2004, Case Western Reserve University.
8. Osswald, T.A. and G. Menges, *Materials science of polymers for engineers*. 2012: Carl Hanser Verlag GmbH Co KG.
9. Yamada, C. *New functionalised SSBR types for overall improved tire performance*. in *Tire Technology Expo Conference*. 2018. Hannover Germany.
10. Xu, X., et al., *Studies on the steady and dynamic rheological properties of poly(dimethyl-siloxane) filled with calcium carbonate based on superposition of its relative functions.* Journal of Applied Polymer Science, 2008. **107**(3): p. 1590-1597.
11. Barnes, H.A., *A REVIEW OF THE RHEOLOGY OF FILLED VISCOELASTIC SYSTEMS.* 2003.
12. Mark, J.E., B. Erman, and M. Roland, *The science and technology of rubber*. 2013, Elsevier Academic Press: Amsterdam ;.
13. Bayram, G., Ü. Yilmazer, and N. Orbey, *Viscoelastic properties of suspensions with weakly interacting particles.* Journal of Applied Polymer Science, 1998. **70**(3): p. 507-514.
14. Tassieri, M. and M.C.A.A.C.i.c.o.r.S.o.R.a.m.M.C. Conference: 15. international congress on rheology: Society of Rheology 80. annual meeting, *A Study of the Rheology, Processing and Flow Induced Mesostructures of Glass Bead Filled Polystyrene.* AIP Conference Proceedings, 2008. **1027**(1): p. 105-107.
15. Krishnamoorti, R., J. Ren, and A.S. Silva, *Shear response of layered silicate nanocomposites.* The Journal of Chemical Physics, 2001. **114**(11): p. 4968-4973.
16. Robertson, C.G., R. Bogoslovov, and C.M. Roland, *Effect of structural arrest on Poisson's ratio in nanoreinforced elastomers.* Physical Review E, 2007. **75**(5): p. 051403.
17. Cassagnau, P., *Payne effect and shear elasticity of silica-filled polymers in concentrated solutions and in molten state.* Polymer, 2003. **44**(8): p. 2455-2462.
18. Yamada, S., et al., *Analytical and Experimental Evaluation of Dispersive Mixing Performance of Special Rotor Segments in a Corotating Twin-Screw Extruder.* Polymer - Plastics Technology and Engineering, 2016. **55**(15): p. 1577-1585.
19. Yamada, S., et al., *Dispersive mixing performance evaluation of special rotor segments in an intermeshing co-rotating twin-screw extruder by using weighted probability distributions.* International Polymer Processing, 2015. **30**(4): p. 451-459.
20. Xu, B., et al., *Evaluation of Mixing Performance in Baffled Screw Channel Using Lagrangian Particle Calculations.* Advances in Polymer Technology, 2017. **36**(1): p. 86-97.
21. Hopmann, C., et al., *Analysis of mixing behavior of pin barrel extruders by means of simulative and experimental methods.* KGK Kautschuk Gummi Kunststoffe, 2016. **69**(5): p. 30-36.
22. Chen, J. and Y. Cao. *Simulation of 3D flow field of RPVC in twin-screw extrusion under wall slip conditions*. in *Proceedings of 2012 9th International Bhurban Conference on Applied Sciences and Technology, IBCAST 2012*. 2012.
23. Xie, H.L., et al., *Numerical Simulation of Mixing Characteristics and Energy Consumption in Vane Extruders with Different Structure Parameters.* Journal of Macromolecular Science, Part B: Physics, 2017. **56**(6): p. 395-408.
24. Zong, Y., H. Tang, and L. Zhao, *3-D numerical simulations for polycondensation of poly(p-phenylene terephthalamide) in twin screw extruder.* Polymer Engineering and Science, 2017. **57**(11): p. 1252-1261.

25. Lattuada, M., et al., *Kinetic modeling of aggregation and gel formation in quiescent dispersions of polymer colloids.* Macromolecular Symposia, 2004. **206**(1): p. 307-320.
26. Somasundaran, P. and V. Runkana, *Modeling flocculation of colloidal mineral suspensions using population balances.* International Journal of Mineral Processing, 2003. **72**(1): p. 33-55.
27. Grimard, J., L. Dewasme, and A. Vande Wouwer, *A Review of Dynamic Models of Hot-Melt Extrusion.* Processes, 2016. **4**(2).
28. Wang, L., et al., *CFD simulation of aggregation and breakage processes in laminar Taylor–Couette flow.* Journal of Colloid and Interface Science, 2005. **282**(2): p. 380-396.
29. Marchisio, D.L., et al., *Role of turbulent shear rate distribution in aggregation and breakage processes.* AIChE Journal, 2006. **52**(1): p. 158-173.
30. Tucker, C., *Mixing of Miscible Liquids*, in *Mixing and Compounding of Polymers*. 2009, Carl Hanser Verlag GmbH & Co. KG. p. 5-39.
31. Tang, H., Y. Zong, and L. Zhao, *Numerical simulation of micromixing effect on the reactive flow in a co-rotating twin screw extruder.* Chinese Journal of Chemical Engineering, 2016. **24**(9): p. 1135-1146.
32. Zhang, X.M., et al., *Assessing local residence time distributions in screw extruders through a new in-line measurement instrument.* Polymer Engineering & Science, 2006. **46**(4): p. 510-519.
33. Zhang, X.M., et al., *Local residence time, residence revolution, and residence volume distributions in twin-screw extruders.* Polymer Engineering & Science, 2008. **48**(1): p. 19-28.
34. Zhang, X.M., et al., *Numerical simulation and experimental validation of mixing performance of kneading discs in a twin screw extruder.* Polymer Engineering & Science, 2009. **49**(9): p. 1772-1783.
35. Manas-Zloczower, I., et al., *Color Mixing in Extrusion: Simulations and Experimental Validation*, in *NSF DMII Grantees Conference*. 2005: Scottsdale Arizona, USA.
36. Alemaskin, K., I. Manas-Zloczower, and M. Kaufman, *Color mixing in the metering zone of a single screw extruder: numerical simulations and experimental validation.* Polymer Engineering & Science, 2005. **45**(7): p. 1011-1020.
37. Alemaskin, K., I. Manas-Zloczower, and M. Kaufman, *Entropic analysis of color homogeneity.* Polymer Engineering & Science, 2005. **45**(7): p. 1031-1038.
38. Alemaskin, K., et al. *Entropic measures of mixing tailored for various applications*. in *AIP Conference Proceedings*. 2004. AIP.
39. Alemaskin, K., et al. *Entropic mixing characterization in a single screw extruder*. in *SPE ANTEC*. 2004.
40. Alemaskin, K., I. Manas–Zloczowe, and M. Kaufman, *Index for simultaneous dispersive and distributive mixing characterization in processing equipment.* International Polymer Processing, 2004. **19**(4): p. 327-334.
41. Alemaskin, K., I. Manas-Zloczower, and M. Kaufman. *Simultaneous characterization of dispersive and distributive mixing in a single screw extruder*. in *Proceedings of the Int. Conf. ANTEC*. 2003.
42. Buist, J., et al., *Polymer Mixing in a Single Screw Extruder (Part 2: Mixing quantification)*. Windesheim, LKT-DP-106741-2305, 2023.
43. Meijer, H.E.H., J.M.H. Janssen, and P.D. Anderson, *Mixing of Immiscible Liquids*, in *Mixing and Compounding of Polymers*. 2009, Carl Hanser Verlag GmbH & Co. KG. p. 41-182.
44. Utracki, L.A. and C.A. Wilkie, *Polymer blends handbook*. Vol. 1. 2002: Springer.
45. Dealy, J.M. and K.F. Wissbrun, *Melt rheology and its role in plastics processing: Theory and applications.* New York: Van Nostram Reynhold, 1990.
46. Grace†, H.P., *DISPERSION PHENOMENA IN HIGH VISCOSITY IMMISCIBLE FLUID SYSTEMS AND APPLICATION OF STATIC MIXERS AS DISPERSION DEVICES IN SUCH SYSTEMS.* Chemical Engineering Communications, 1982. **14**(3-6): p. 225-277.
47. Bazhlekov, I.B., P.D. Anderson, and H.E.H. Meijer, *Nonsingular boundary integral method for deformable drops in viscous flows.* Physics of Fluids, 2004. **16**(4): p. 1064-1081.
48. Janssen, J.M.H. and H.E.H. Meijer, *Dynamics of liquid-liquid mixing: A 2-zone model.* Polymer Engineering & Science, 1995. **35**(22): p. 1766-1780.

49. Dubbelboer, A., et al., *Population balances combined with Computational Fluid Dynamics: A modeling approach for dispersive mixing in a high pressure homogenizer.* Chemical Engineering Science, 2014. **117**: p. 376-388.
50. Tang, H., H. Tang, and L.C. Wrobel, *Modelling the interfacial flow of two immiscible liquids in mixing processes.* International journal of engineering science, 2005. **43**(15): p. 1234-1256.
51. *Marlex® TRB-432 Polyethylene HIGH DENSITY POLYETHYLENE (HDPE)*.
52. Vats, S., *STUDIES ON MELT RHEOLOGICAL CHARACTERISTICS OF LINEAR POLYOLEFINS USING UHMW-PE AS AN ADDITIVE*. 2012.
53. Patterson, S.E. and M.A. Spalding, *Molecular Design of High Density Polyethylene for Pipes*, in *Pipelines 2012: Innovations in Design, Construction, Operations, and Maintenance, Doing More with Less*. 2012. p. 964-973.
54. Molina-Aiz, F., et al., *Comparison of finite element and finite volume methods for simulation of natural ventilation in greenhouses.* Computers and electronics in agriculture, 2010. **72**(2): p. 69-86.
55. Zienkiewicz, O.C., R.L. Taylor, and P. Nithiarasu, *The finite element method for fluid dynamics*. 2005: Spain: Elsevier; ISBN 0-7506-6322-7.
56. Versteeg, H.K. and W. Malalasekera, *An introduction to computational fluid dynamics: the finite volume method*. 2007: Pearson education.
57. McNaughton, J., et al., *A simple sliding-mesh interface procedure and its application to the CFD simulation of a tidal-stream turbine.* International Journal for Numerical Methods in Fluids, 2014. **74**(4): p. 250-269.
58. Blades, E.L. and D.L. Marcum, *A sliding interface method for unsteady unstructured flow simulations.* International Journal for Numerical Methods in Fluids, 2007. **53**(3): p. 507-529.
59. Jendoubi, A., et al., *An immersed boundary method for fluid flows around rigid objects.* International Journal for Numerical Methods in Fluids, 2014. **75**(1): p. 63-80.
60. Ilinca, F. and J.F. Hétu, *Solution of flow around complex-shaped surfaces by an immersed boundary-body conformal enrichment method.* International Journal for Numerical Methods in Fluids, 2012. **69**(4): p. 824-841.
61. Park, J.W., J.W. Hwang, and Y.H. Kim, *Efficient finite element analysis using mesh superposition technique.* Finite Elements in Analysis and Design, 2003. **39**(7): p. 619-638.
62. Buist, J., D.J. Van Dijk, and T.J. Mateboer, *TIRE RUBBER EXTRUDATE SWELL SIMULATION AND VERIFICATION WITH EXPERIMENTS*, in *12th International Conference on CFD in Oil and Gas, Metallurgical and Process Industries*. 2017: Trondheim, Norway.

Professorship for Polymer Engineering

Polymer Mixing in a Single Screw Extruder

Part I: Simulation Method

About this Professorship

The Professorship for Polymer Engineering of University of Applied Sciences Windesheim was founded in 2009; the group's objective is to improve the knowledge base on sustainable processing of plastics and composites within and through the higher education system. Its primary function is as a research group in Polymer Engineering, delivering output in the field of applied science. The team operates within market based projects and comprises lecturers from Civil Engineering, Industrial Product Design and Mechanical Engineering. The output of the projects is integrated into the curriculum of these study programs.

Summary

In this TechForFuture project 'Polymer Mixing in a Single Screw Extruder' a method to optimize mixing elements is developed based on numerical simulations (Computational Fluid Dynamics, CFD). A numerical procedure is developed to calculate the flow field in the extruder. By tracing particles in this field data is collected to determine distributive and dispersive mixing. Based on these data measuring values, the so called resident time distribution and Shannon entropy, have been used to quantity mixing. This way numerical values can be compared to experimental values such that the developed procedure could be validated with experiment on a single screw extruder on labscale with different mixing elements. In the end, this numerical procedure can be used to analyze, optimize and judge different mixing elements with respect to their performance. The work has been carried out in close collaboration with Wavin T&I.

University of Applied Sciences Windesheim